AD-A086 860 NAVAL SURFACE WEAPONS CENTER WHITE OAK LAB SILVER SP--ETC F/G 20/14
SINGULARITY EXTRACTION OF EMP RESPONSE WAVEFORMS BY PRONY'S MET--ETC(U)
MAY 80 A S LEVECKIS
UNCLASSIFIED NSWC/WOL/TR-77-99 NL

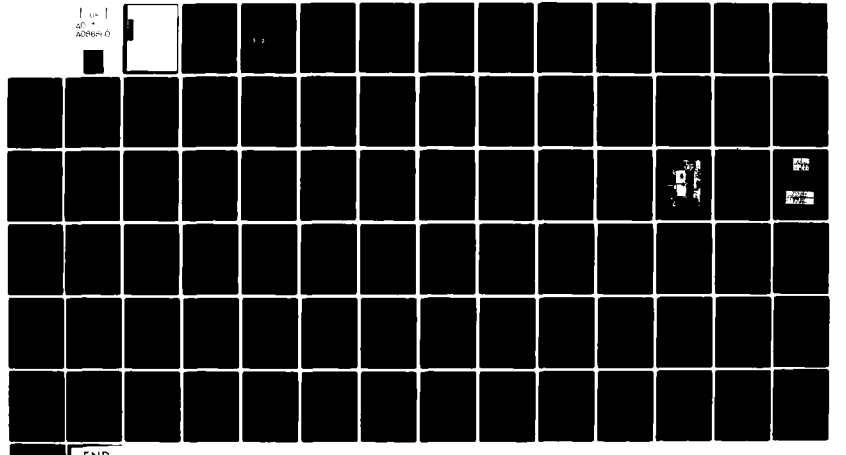

END
DATE FILMED
8-80
DTIC

UNCLASSIFIED

SECURITY CLASSIFICATION OF THIS PAGE *(When Data Entered)*

REPORT DOCUMENTATION PAGE

READ INSTRUCTIONS BEFORE COMPLETING FORM

1. REPORT NUMBER: NSWC/WOL/TR-77-99
2. GOVT ACCESSION NO.: AD-A086 860
3. RECIPIENT'S CATALOG NUMBER:

4. TITLE (and subtitle): SINGULARITY EXTRACTION OF EMP RESPONSE WAVEFORMS BY PRONY'S METHOD.
5. TYPE OF REPORT & PERIOD COVERED: Final rept.
6. PERFORMING ORG. REPORT NUMBER:

7. AUTHOR(s): Algis S. Leveckis
8. CONTRACT OR GRANT NUMBER(s):

9. PERFORMING ORGANIZATION NAME AND ADDRESS: Naval Surface Weapons Center, Silver Spring, MD 20910
10. PROGRAM ELEMENT, PROJECT, TASK AREA & WORK UNIT NUMBERS: 62734N; ZF34-384-001

11. CONTROLLING OFFICE NAME AND ADDRESS: Naval Surface Weapons Center, Silver Spring, MD 20910
12. REPORT DATE: May 1980
13. NUMBER OF PAGES: 86

14. MONITORING AGENCY NAME & ADDRESS *(if different from Controlling Office)*:
15. SECURITY CLASS. *(of this report)*: UNCLASSIFIED
15a. DECLASSIFICATION/DOWNGRADING SCHEDULE:

16. DISTRIBUTION STATEMENT *(of this Report)*

Approved for public release; distribution unlimited.

17. DISTRIBUTION STATEMENT *(of the abstract entered in Block 20, if different from Report)*

18. SUPPLEMENTARY NOTES

19. KEY WORDS *(Continue on reverse side if necessary and identify by block number)*

Prony
Singularity Expansion Method
Nyquist Criterion
EMP
Sempex

20. ABSTRACT *(Continue on reverse side if necessary and identify by block number)*

The Singularity Expansion Method has grown from a theoretical idea to a numerical technique that calculates the poles of a given scattering object. It has spawned the study and growth of Prony's method, which calculates the poles of the scattering object, from the scatter field that is in response to an incident electromagnetic wave. Here is presented the results of an attempt to use Prony's method on EMP response waveforms on ships. The technique to acquire the experimental data is detailed; the numerical problem is

DD FORM 1 JAN 73 1473 EDITION OF 1 NOV 65 IS OBSOLETE
S/N 0102-LF-014-6601

UNCLASSIFIED

SECURITY CLASSIFICATION OF THIS PAGE *(When Data Entered)*

391596

20. ABSTRACT (Continued)

posed, and the goals are quickly simplified to attempting to find the best curve-fit to the waveform, using complex exponentials, and then hoping to eliminate the curve-fit poles. A method is presented that aids in the "physical pole" selection process, and explained also is the significance of the right half plane poles in the results.

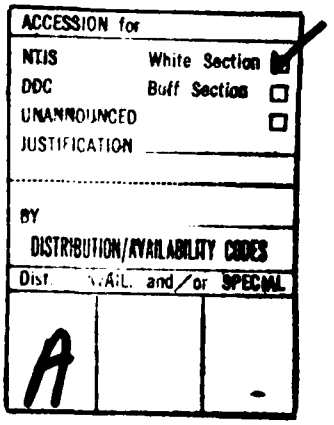

PREFACE

The study of EMP responses, has as of late, become a numerical procedure, and recently in the technique called Singularity Expansion, a new method has been proposed which evaluates the poles and residues of any response waveform. The goal is that these calculated poles be easily related to the physical structure of the scattering/receiving structure. This report explores an area of use for one of these methods - Prony's method. It examines the possibility of using the Prony technique on EMP response waveforms, where the scattering object is a complicated structure.

Chapter 1 discusses the reasons that SEM may be of interest in ship EMP response analysis. Chapter 2 provides background in SEM and the Prony technique. Chapter 3 presents the computer code that is based on the Prony method and describes its use. Chapter 4 describes the EMPRESS EMP simulation facility, and presents a summary of the experimental work conducted. Chapter 5 introduces a technique that aids in the elimination of the "curve fit" poles from the calculated results. In addition, the process of the data anlaysis is described.

I would especially like to thank the following people for their help and valuable comments during the course of the work. Professor Jin A. Kong, MIT Advisor; Dr. M. L. VanBlaricum of Mission Research Corporation, Santa Barbara, California; Mary Laanisto, Neal Stetson, George Brackett, and Robert Baran, all of the Naval Surface Weapons Center, White Oak Laboratory, Silver Spring, Maryland. The results of this research were submitted to the Department of Electrical Engineering and Computer Science, Massachusetts Institute of Technology, Cambridge, Massachusetts in partial fulfillment of the requirements for the degree of Master of Science.

Released by:

D. B. COLBY, Head
Electronics Systems Department

CONTENTS

ILLUSTRATIONS

TABLES

Chapter 1

EMP AND SHIP COUPLING

1.1 EMP

Nuclear weapons effects have for a long time been a major consideration in military systems research and development. It was only in the 1960's that the nuclear weapons effect known as the electromagnetic pulse (EMP) was identified as a potentially harmful phenomenon, especially in the case of a high altitude burst (HAB). After an HAB, when a high yield nuclear weapon is detonated above the ionosphere, the only significant effect on the earth's surface is this EMP. All other effects, such as the shock wave, the heat wave, and the radiation are absorbed by the atmosphere. Today the study of EMP effects is very important, since most electronic equipment utilizes semiconductor components. State-of-the-art integrated circuit equipment, unlike vacuum tube devices, can be extremely vulnerable to any type of transients. Transients can cause upset, or even destruction, if the transients exceed the normal use or breakdown specifications. The increasing sophistication in nuclear strategy and armament, puts much more emphasis now on the hardening of defense systems against nuclear effects, including EMP. It has been theorized by the Defense Nuclear Agency[1], that an HAB could give an attacking force as much as a thirty minute advantage, by upsetting or destroying electronic devices in parts of the defense system.

1.2 EMP COUPLING

Ways in which EMP can couple into electronic equipment on a ship are shown in Figure 1.1. Pathways I are the primary means of EMP coupling to the ship's systems. The pulse itself is not detectable on most waveforms taken on a ship; it may appear only in making the first peak of a waveform a little higher than would be expected. On a ship, the effect of pseudo-focusing is common due to the large structures with high amplitude resonant currents. The presence of the original EMP would be unascertainable in such a waveform. All pathways down the II section are almost insignificant. The amount of energy coupled down these paths depends on the amplitudes of the resonances of the skin current in the vicinity of the aperture, the size of the aperture, and the size of the room. The apertures can be modeled by infinitesimal or large dipole current

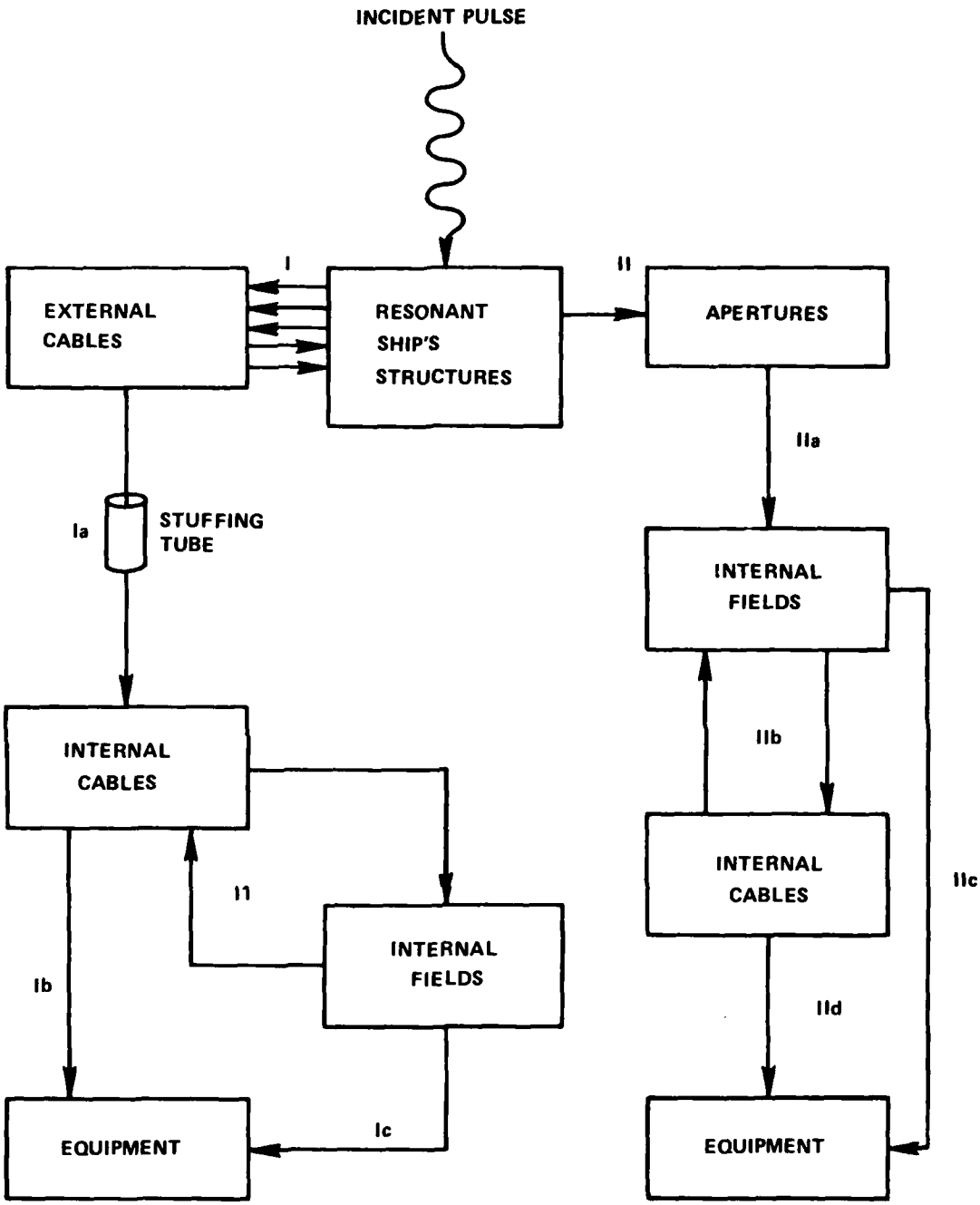

FIG. 1.1 EMP COLLECTOR FLOWPATHS IN A SHIP

sources depending on the size of the window. In a test that was conducted in the largest room with the largest apertures on a ship, it was found that the internal fields caused by aperture coupling were insignificant except very close to the aperture. Thus the energy in pathways IIb and IId is small and only in IIc could it become significant if the equipment is very near large windows. In pathway I the resonant ship structures have high amplitude currents and by radiation couple to other ship's structures and external cables. The worst case can be found in cables that are routed up the mast. The external cables then pass through the deck of the ship and radiate fields into the internal compartments, Figure 1.2. Good grounding techniques between the external cable and the stuffing tube through the deck (Ia of Figure 1.1) have been shown to attenuate the internal fields, but do not eliminate the problem. The energy in the internal cables couples to other internal cables via the I1 loop. The internal fields that are part of the loop, could affect equipment via path Ic. Field tests have shown that the internal cables that originate on the mast still radiate high amplitude electromagnetic fields even several decks below, before finally reaching the equipment by path Ib. This is the most serious case in EMP penetration into ship's equipment.

1.3 BACKGROUND FOR SEM ANALYSIS FOR SHIPS

The resonant currents on the ship's structures and cables show damped oscillations. These oscillations correspond to the natural modes of the current on the structure that are the solutions to the integral equations describing the current for the structure. They can be represented as a sum of complex exponentials, with the exponent, ($s = \sigma + j\omega$) termed a pole, specifying a pole location on the complex s-plane. The location of the poles is only a function of the physical properties of the structure involved. The coefficients of the complex exponentials are the complex residues at each pole location in the s-plane or the "coupling coefficients" times the natural modes, since they depend on the form of the exciting waveform[3]. The Prony method of Singularity Expansion Method (SEM) determines the poles and the coupling coefficients for the EMP transient response waveform, which should be the poles of the resonating structure(s). Thus, it is actually extracting poles from a waveform, the reverse of the expansion process. Interest in this method was brought about by the presence and dominance of the ship structures' resonating currents in most data taken on a ship.

Interest in SEM at the Naval Surface Weapons Center (NSWC) grew out of several ongoing projects. One was a study of antenna equivalent circuits. This was based on a Illinois Institute of Technology Research Institute (IITRI) feasibility study[4], using the reciprocity of antennas to predict the full-threat level EMP response. The technique is to calculate the equivalent circuit of the antenna,

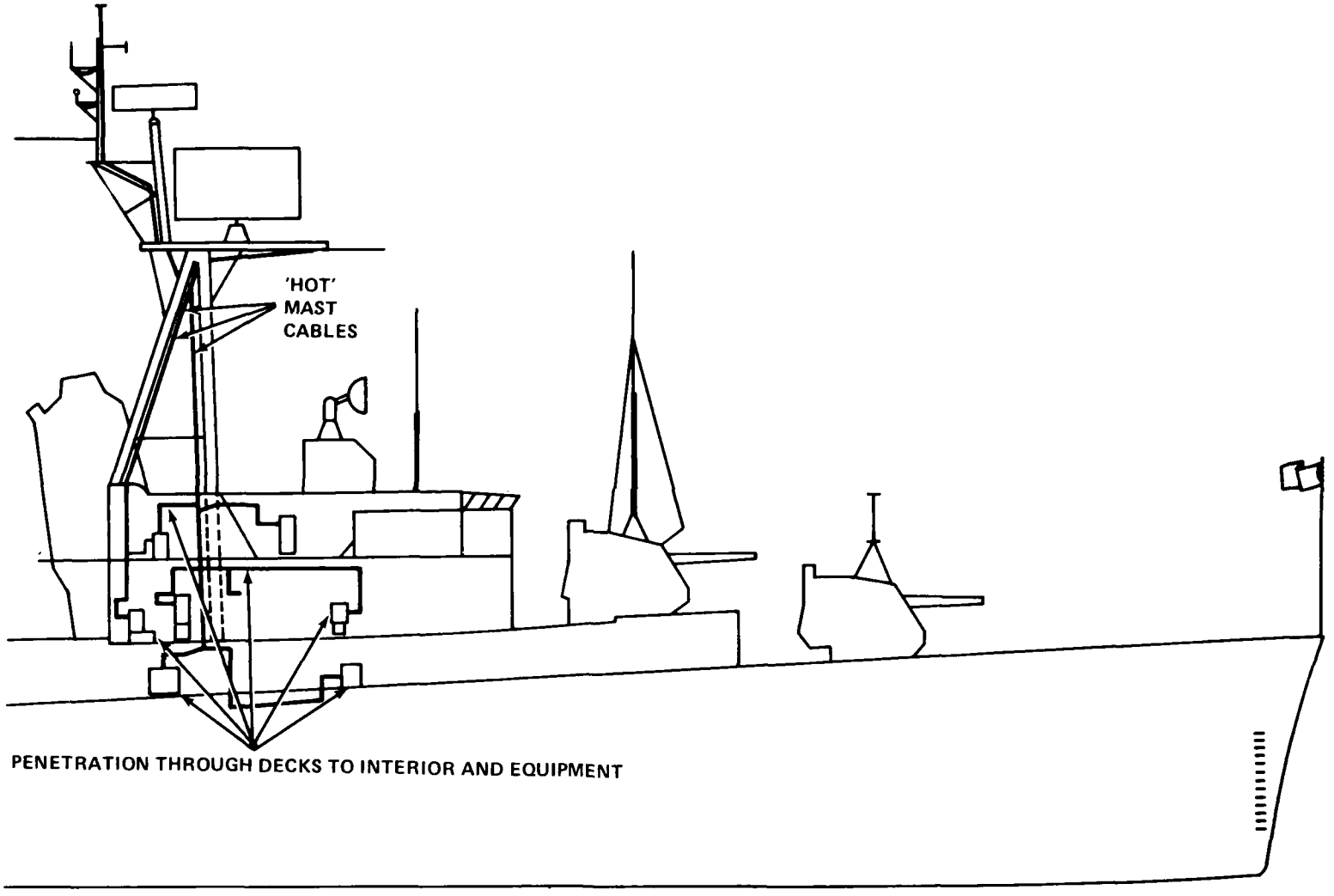

FIG. 1.2 HIGH AMPLITUDE CURRENT CARRYING MAST CABLES

in its environment, by exciting the antenna at the base with a pulse injection source and simultaneously measuring the radiated electric field. Using the equivalent circuit obtained by this method it would then be a simple matter to compute the response of the antenna to any excitation. The method is cumbersome and could be simplified by representing the antenna response by a set of poles, extracted by SEM. Another project for which SEM seemed to have an answer was the design of injection sources for full-threat level testing. Here the EMP response of the antenna system, the antenna in its environment, the cable routing, all intercoupling between the cables, would be measured at the input to the equipment. After calculating the poles of the system from the response, it would be possible to design a damped sinewave injection source that could reproduce the waveform, but at full threat level. A new project which provided the motivation for this thesis, was to examine the pole locations of antennas, with respect to their locations on the ship. It thereby would be possible to identify the structures that contribute the most to a specific antenna's response.

The results of an SEM analysis of a response waveform would provide much information on the antenna, and the antenna system's environment. Concrete answers might make it possible to redesign the ship's superstructure, or simply place antennas in a more optimum location to reduce the coupling from structures with high resonant currents. With the identification of the structures, they could also be included in theoretical models to provide more realistic predictions for ship systems' EMP responses.

Chapter 2

METHODS OF POLE CALCULATION

2.1 PREVIOUS METHODS

Previous to today's quick numerical methods of SEM much analysis had been done to find the natural frequencies of many objects. The first attempt seems to be attributed to Pocklington[5] who constructed the integro-differential equation for current, and solved it for the first mode of a small thin ring. He also was able to derive the first mode coupling coefficients[6] for a wave incident upon the ring on its axis. Oseen[7] and Hallen[8] derived natural frequencies for thin wires. Oseen applied the method of retarded potentials to thin wires, and derived asymtotic formulas for the natural frequencies. Hallen derived a pure integral equation for current on a wire, and was able to solve for the weakly damped modes. K. K. Mei extended the Hallen integral equation to include thin wire antennas of arbitrary geometry. In the past years, much of the research effort has been geared to the formulation of numerical methods of solution to the integral equations, though the analytical technique was recently revived and expanded by L. Marin[9]. He adapted the Hallen integral equation for electric field formulation and analytically determined the approximate fields for scattering from several thin wire structures. He concedes that the analytical approach is feasible for the location of the natural modes to represent the late and possibly the intermediate times of an impulse response, due to the small number of poles needed to accomplish this, and because poles in the weakly damped part of the spectrum are easier to find. He leaves the calculation of poles to represent the early times of a waveform to numerical techniques. Marin[10] constructed a numerical technique to solve the magnetic field integral equation to find some of the poles of the prolate spheroid. He reduced the integral equation to two sets of coupled one dimensional integral equations and then solved these numerically. Miller, Poggio, and Burke[11] developed a numerical method to solve the electric field integral equation for thin wires. In addition, they suggested that the magnetic field integral equation is best used for the analysis of solid surfaces, while the electric field formulation is better for the solution of thin wire problems.

2.2 TESCHE'S METHOD AND SEM

Carl Baum[12] presented the Singularity Expansion technique for the general problem of electromagnetic scattering from finite conducting bodies, in defining the natural frequencies, modes, and coupling coefficients. F. Tesche[13] developed a technique to numerically calculate the poles and coupling coefficients for thin wire structures. Knowing these parameters makes it much simpler to calculate the response due to any excitation at any incident angle; just as in circuit theory, knowing the impulse response, the poles of the circuit, it is easy to calculate the response to an arbitrary excitation. Previously, using the time harmonic analysis with Fourier inversion, it was necessary to recalculate almost the entire problem to find the response when just the angle of incidence changed. Here, using the method of moments[14], an electric field integro-differential equation is transformed into a matrix equation, where the zeroes of the determinant of the system "impedance" matrix are the natural frequencies ($s = \sigma + j\omega$) of the system. For each of the natural frequencies, there is a residue matrix, which in the electric field case can be defined by two vectors, which are identical.

Consider a wire of length L and diameter a, whose axis is coincident with the z axis in (z,ϕ,θ) space. A step function wave-front is incident from the negative z direction and encounters the wire at $z = 0$ and $t = 0$. An integro-differential equation can be written for the z-directed current $I(z,s)$. Starting with a general integral equation

$$-\underline{\underline{\mathfrak{L}}} \cdot \underline{J} = -s\epsilon_o \underline{E}_t \tag{2.1}$$

with the integral operator defined by

$$-(\underline{\underline{\mathfrak{L}}} \cdot \underline{J})(\underline{r}) = \left(\nabla\nabla - \frac{s^2}{c^2}\right) \int_S G(\underline{r},\underline{r}',s) \cdot \underline{J}(\underline{r}')\, ds' \tag{2.2}$$

where $G(\underline{r},\underline{r}',s)$ is the free space Green's function

$$G(\underline{r},\underline{r}',s) = \frac{1}{2\pi} \frac{1}{(4\pi\,|\underline{r}-\underline{r}'|)} e^{-\frac{s|\underline{r}-\underline{r}'|}{c}} \tag{2.3}$$

and s is the complex natural frequency

c is the speed of light

$\underline{E}_t(z,s)$ is the incident tangential electric field

$$\underline{E}_t(z,s) = \underline{E}_i(s) \sin\theta \, e^{-\frac{sz\cos\theta}{c}} \tag{2.4}$$

where for a step wave, in the s-domain

$$\underline{E}_i(s) = \frac{E_o}{s} \tag{2.5}$$

By assuming that there is no ϕ variation, equation (1.1) can be rewritten

$$(-sE_o\underline{E}_t(z,s)) = \int_0^L \underline{I}(z,s) \left(\frac{\partial^2}{\partial z^2} - \frac{s^2}{c^2} \right) K(z,z',s) \, dz' \tag{2.6}$$

where $K(z,z',s)$ is the kernel of the equation defined by

$$K(z,z',s) = \frac{1}{2\pi} \int_0^{2\pi} e^{-\frac{sR}{c}} \frac{1}{4\pi R} \, d\phi \tag{2.7}$$

and the point of observation R is

$$R = \sqrt{|z-z'|^2 + a^2 \sin^2 \frac{\theta}{2}} \tag{2.8}$$

Previous methods solved equation (2.6) for many $j\omega$ and then Fourier inverted for the time-domain response. In Tesche's analysis, the technique is to find the poles of the current function $\underline{I}(z,s)$ in the s-plane in a manner similar to circuit analysis, i.e., let the incident electric field be zero and find the non trivial solutions to the homogeneous integro-differential equation. The equation can be transformed by the method of moments to a matrix equation

$$(Z(s)) \, (I(s)) = (V(s)) \tag{2.9}$$

$(Z(s))$ the impedance matrix is a square n x n matrix, $(I(s))$ is the current response vector, and $(V(s))$ the voltage or source vector, both of dimension n. Now $(V(s))$ is set to zero and the non trivial solutions will be those s_j such that

$$\det (Z(s)) = 0 \tag{2.10}$$

Solving equation (2.9) for the response vector

$$(I(s)) = \frac{(Y(s))}{\det\ (Z(s))}\ (V(s)) \tag{2.11}$$

and then by Fourier inversion one obtains the current time response

$$(i(t)) = \frac{1}{2\pi j} \int_{\sigma_o - j\omega}^{\sigma_o + j\omega} \frac{(Y(s))}{\det\ (Z(s))}\ (V(s))\ e^{st}\ ds \tag{2.12}$$

now let

$$\frac{(Y(s))}{\det\ (Z(s_i))} = \sum_i \frac{R_i}{s - s_i} \tag{2.13}$$

This is the sum over all the poles in the complex s-plane, and (R_i) is the residue matrix. This matrix is a dyadic and can be represented by the outer product of two vectors of dimension n: (M_i) the natural mode vector, and $(C_i)^T$ where (C_i) is the coupling vector, where the vectors are the solutions of the following equations respectively

$$(Z(s_i))\ (M_i) = 0 \tag{2.14}$$

$$(Z(s_i))^T\ (C_i) = 0 \tag{2.15}$$

In the electrical field formulation these vectors are identical and therefore

$$(R_i) = (C_i)\ (C_i)^T \tag{2.16}$$

now with (V(s)) represented as a step function in the s-domain $(V_o(s))/s)$

$$i(t) = \frac{1}{2\pi j} \int_{\sigma_o - j\omega}^{\sigma_o + j\omega} \frac{(C_i)(C_i)^T}{s - s_i}\ \frac{V_o(s)}{s}\ e^{st}\ ds \tag{2.17}$$

which can be rewritten into

$$i(t) = \frac{1}{2\pi j} \int \sum \frac{(C_i)(C_i)^T}{s_i(s-s_i)} V_o(s)\, e^{st} - \sum \frac{(C_i)(C_i)^T}{s\, s_i} V_o(s)\, e^{st}\, ds \qquad (2.18)$$

Interchanging the orders of summation and integration, and closing the contour on $s = \sigma_o$ at infinity, the integrals can be evaluated by the Cauchy Intergral formula[15].

$$i(t) = \sum_i (C_i)(C_i)^T \underline{U}(t) \frac{(V_o(s_i))}{s_i} - \sum_i \frac{(C_i)(C_i)^T}{s_i} \underline{U}(t)\, (V_o(0)) \qquad (2.19)$$

where $\underline{U}(t)$ is a diagonal matrix of unit step functions which becomes the identity matrix after the wavefront of the incident wave has completely passed the structure at $z = L$, i.e., for $t > L/c$. The last sum of the equation (2.19) must be zero because the response for the late times must decay to zero, and this term is time dependent. Now

$$i(t > L/c) = \sum_i (C_i)(C_i)^T (V_o(s_i)) \frac{1}{s} e^{s_i t} \qquad (2.20)$$

This is just a sum of damped sinusoids. Baum has defined a coupling coefficient η

$$\eta_i = (C_i)^T (V_o(s_i)) \qquad (2.21)$$

such that $\nu_i = C_i$, the mode vector, is the only term dependent upon the incident field

$$i(t) = \nu_i\, \eta_i\, e^{s_i t/s_i} \qquad (2.22)$$

In the numerical search procedure to find the pole locations, i.e., the solutions to equation (2.10), the determinant of the system impedance matrix is regarded as a complex function. It is expanded in a Taylor series and only the first two terms are kept to obtain

$$(s_i - s_o) = - \frac{\det\ (Z(s_o))}{\frac{d}{ds} \det\ (Z(s_o))} \tag{2.23}$$

An initial guess must be made for the pole, then by an iterative process similar to the Newton-Raphson method for real functions, the pole locations are calculated. The residue at each pole s_k is found by evaluating

$$(R_k) = \lim_{\varepsilon \to o} \varepsilon\ [z(s_k+\varepsilon)]^{-1} \tag{2.24}$$

where $s = s_k + \varepsilon$ for small enough ε such that the value of (R_k) does not change, and

$$(R_k) = \lim_{s \to s_k} (s-s_k) \sum_i \frac{R_i}{s-s_i} = \lim_{s \to s_k} (s-s_k)\ (Z(s))^{-1} \tag{2.25}$$

where $(Z(s))^{-1}$ becomes undefined at $s = s_k$. Tesche calculated the poles for thin wire and a sphere, compared them with previous results and showed the simplicity of recalculating the time-domain response for different angles of the incident wavefront.

2.3 THE PRONY METHOD FOR SINGULARITY EXTRACTION

In 1974, Van Blaricum and Mittra[16] presented a new technique for locating the poles of objects. Their method was based on the premise that if the transient response can be calculated from the poles, then the poles can be determined from the transient response. Van Blaricum[17] formalized and expanded the procedure that is based on Prony's algorithm[18,19] which represents a signal in terms of complex exponentials. The derivation of the Prony technique is presented here.

Given that it is possible to represent a waveform by a sum of damped sinusoids, an impulse response for the electromagnetic scattering of an object can be defined

$$H(\underline{r},s) = \sum_{i=1}^{\infty} \eta_i(s,\underline{p})\nu_i[s-s_i]^{-1} \tag{2.26}$$

where $\underline{p}$ is the polarization of the incident wave

and in the time domain

$$H(\underline{r},t) = U(t-t_o) \sum_{i=1}^{\infty} \eta_i(s,\underline{p})\nu_i \, e^{s_i t} \tag{2.27}$$

where $t_o > 0$, due to the presence of the impulse exciter at $t = 0$, since the impulse function cannot be represented by a sum of complex exponentials. Thereby, knowing the impulse response, the response R(s), due to an arbitrary function F(s) is then simply found by

$$R(s) = F(s)\, H(s) \tag{2.28}$$

Then the time domain response R(t) is retrieved by an inverse Laplace transform, exactly as in circuit theory. R(t) can be any function that can be acquired experimentally, and will have the form

$$R(t) = \sum_{i=1}^{N} A_i \, e^{s_i t} \tag{2.29}$$

where A_i is defined as the residue at the pole s_i. Here as opposed to equations (2.26) and (2.27), the summation is truncated at N, since realistically any waveform that can be generated is bandlimited, and can contain only a finite number or poles. The waveform will be digitized and then can consist of M discrete equally spaced samples.

$$R(\tau_m) = R_m = \sum_{i=1}^{N} A_i \, e^{s_i m\Delta t} \qquad m = 0,1,2\ldots M-1 \tag{2.30}$$

where $\tau_m = m\Delta t$ is the time of the $R_m{}^{th}$ data sample, and Δt is the spacing between the samples. Equation (2.30) is actually representative of M nonlinear equations in 2N unknowns, and can be rewritten in the expanded form

$$R_o = A_1X_1{}^0 + A_2X_2{}^0 + A_3X_3{}^0 + \ldots\ldots\ldots + A_NX_N{}^0 \tag{2.31.0}$$

$$R_1 = A_1X_1{}^0 + A_2X_2{}^0 + A_3X_3{}^0 + \ldots\ldots\ldots + A_NX_N{}^0 \tag{2.31.1}$$

$$\vdots \qquad \vdots \qquad \vdots \qquad \vdots \qquad \vdots \qquad \vdots \qquad \vdots$$

$$R_{M-1} = A_1X_1{}^{M-1} + A_2X_2{}^{M-1} + A_3X_3{}^{M-1} + \ldots\ldots\ldots + A_NX_N{}^{M-1} \tag{2.31.M-1}$$

where

$$X_i = e^{s_i \Delta t} \tag{2.32}$$

It is necessary to solve the equation for the N pole locations and the N values of the residues at the pole locations; therefore, M must be at least 2N to be able to solve the equations. Now let X_is be the solution to the following polynomial

$$\alpha_0 + \alpha_1 X^1 + \alpha_2 X^2 + ... + \alpha_N X^N = 0 \tag{2.33}$$

where the solution to the polynomial can be expressed as

$$(X-X_1)(X-X_2).....(X-X_N) = 0 \tag{2.34}$$

and more simply

$$\sum_{m=0}^{N} \alpha_m X^m = \prod_{i=1}^{N} (X-X_i) = 0 \tag{2.35}$$

To determine the coefficients α_i, equation (2.31.0) is multiplied by α_0, and equation (2.31.1) by α_1 and so on until (2.31.N) is multiplied by α_N. Then the results are summed, and since the X_i are solutions to the polynomial, the sum is also equal to zero.

$$\alpha_0 R_0 + \alpha_1 R_1 + ... + \alpha_N R_N = 0 \tag{2.36}$$

The same procedure is used again, except that this time α_0 multiplies (2.31.1), and α_1 (2.31.2) and so on, and this process is repeated until M-N linear difference equations are obtained

$$\alpha_0 R_0 + \alpha_1 R_1 + ... + \alpha_N R_N = 0 \tag{2.37}$$

$$\alpha_0 R_1 + \alpha_1 R_2 + ... + \alpha_N R_{N+1} = 0$$

$$\alpha_0 R_2 + \quad . \quad . \quad . \quad .$$

$$. \quad . \quad . \quad . \quad .$$

$$. \quad . \quad . \quad . \quad .$$

$$\alpha_0 R_{M-N-1} + \alpha_1 R_{M-N} + ... + \alpha_N R_{M-1} = 0$$

rewritten as

$$\sum_{p=0}^{N} \alpha_p R_{p+k} = 0 \qquad p+k = m = 0,1,2,....M-1 \qquad (2.38)$$

This is called Prony's difference equation where the sampled values R_i satisfy the N^{th} order linear difference equation. Since R_i are known, the equations can be solved for α_i. When $M = 2N$ then the equations are solvable exactly, and if $M > 2N$, the equations can be solved approximately by the least squares method. By normalizing α_N to unity, equation (2.38) can be rewritten in matrix form

$$A\ B = C \qquad (2.39)$$

where

$$A = \begin{bmatrix} R_0 & R_1 & \cdots\cdots\cdots & R_{N-1} \\ R_1 & R_2 & \cdots\cdots\cdots & R_N \\ R_2 & \cdot & \cdot \quad \cdot & \cdot \\ R_{M-N-1} & R_{M-N} & \cdots\cdots\cdots & R_{M-2} \end{bmatrix} \qquad (2.40.A)$$

$$B = \begin{bmatrix} \alpha_0 \\ \alpha_1 \\ \alpha_2 \\ \cdot \\ \cdot \\ \alpha_{N-1} \end{bmatrix} \qquad C = \begin{bmatrix} R_N \\ R_{N+1} \\ R_{N+2} \\ \cdot \\ \cdot \\ R_{M-1} \end{bmatrix} \qquad (2.40.B) \qquad (2.40.C)$$

Then the α_i can be determined by

$$B = (A)^{-1} C \qquad \text{for} \quad M = 2N \qquad (2.41)$$

$$B = (A^T A)^{-1} A^T C \qquad \text{for} \quad M > 2N \qquad (2.42)$$

where matrix A is rectangular, but $(A^T A)$ is square and invertible. The X_is are calculated by finding the roots of equation (2.33), by a polynomial root finding technique. Van Blaricum[17] suggests Muller's method[20], as the "quickest and most accurate". From equation (2.32)

$$s_i = \ln X_i/\Delta t \tag{2.43}$$

The last step is to determine the values of the residues A_i. This involves the solution of equation (2.31) now in matrix form

$$D\ E = F \tag{2.44}$$

Now as with equation (2.41) the A_i are found by

$$E + (D)^{-1}F \tag{2.45}$$

Van Blaricum[17] further shows the relationship between the Prony method and the Corrington difference equation[21], and the Pade approximation[22].

Thus the poles of a system are extracted from the time-domain response waveform making it possible to locate the poles and residues of very complicated structures, without even trying to write the integral equation. Van Blaricum[17] presented his results of trial runs with the Prony method on the response of a 1.0 meter dipole with a half-length to radius ratio of 100, comparing results with those of Tesche[13]. The Prony method poles matched those of Tesche very well and in addition provided more higher frequencies poles and extracted some extra poles that "have been attributed" to the current exciting source.

2.4 FREQUENCY DOMAIN PRONY

Brittingham, Miller, and Willows[23,24,25] derived a procedure for the extraction of poles from real frequency information, which essentially is the Prony method in the frequency domain. Appendix A reproduces a table in reference 23 that shows the similarities of the properties between the time-domain and the frequency-domain Prony techniques. Results on computer generated electromagnetic data proved to be accurate (in relation to the time-domain Prony) though there was a distinct decrease in accuracy in attempting to find the poles in a waveform that contained more than twenty pole pairs.

The experimental data that are acquired in ship field tests are in the time-domain. The method chosen for the work in this report, is the time-domain Prony method as presented by Van Blaricum and Mittra. The other methods, are more suited for such areas as radar target detection and discrimination[25], and the EMP study of structures, such as missiles and airplanes.

CHAPTER 3

THE COMPUTER CODE: SEMPEX

3.1 SIMPLICATIONS FOR ANALYSIS

Using the Prony technique as it stands today, involves several simplifications of the real problem. For one, equation (2.26) should actually contain an entire function in s.

$$H(\underline{r},s) = \sum_{i=1}^{\infty} \eta_i(s,\underline{p})\ \nu_i(s-s_i)^{-1} + W(\underline{r},s) \qquad (3.1)$$

This in the general case is required by the Mittag-Leffler Theorem[27]. According to the theorem, to guarantee the convergence of the infinite series in equation (3.01), each of the pole terms must have an entire function associated with it. The coupling coefficients when defined to be functions of s, as in equation (2.21), have the provision to include an entire function, this is coupled to the fact of whether the coupling coefficient is Class I or Class II, as will be discussed later. The entire function appears from the Laplace transform, and having no singularities in the finite s-plane, it must rise and fall faster than an exponential. The entire function then is limited in influence only to the early-time of a waveform, since the later times are dominated by the complex exponentials. In general the entire function has been neglected in all previous work[28], due to the disinterest in the early-time response and the complexity of the solution.

There have now been defined two types of coupling coefficients, $\eta_i(s)$. The Class I coupling coefficients are the type that are used in Van Blaricum's analyses[17]. This assumes that all the resonances are excited at the same time, i.e., all the damped sinusoids of the complete object start at the same time t=0, exactly when the initial wavefront hits the object. The Class II coefficients are much more difficult to calculate, but give a much better early-time representation. The coefficients in the time-domain are staggered, such that the damped resonances due to structures that have not yet been illuminated by the incident wave do not contribute to the waveform. Hence, the early time response will be much smoother, or less abrupt, when these coefficients are used. For the case of this work, with a ship broadside to the incident field, it would take about

40 nanoseconds for an electromagnetic wave to cross a ship with railing to railing width of about 13 meters. The error that this could produce using Class I coefficients corresponds to stretching a 10 MHz wave, that is 1,000 microseconds long, by 0.040 microseconds, and observing the frequency shift. The worst case would have about a 4% maximum error. For a ship, the major resonant structures are at the center, and the other structures, if any, at the sides of the ship contribute very little for most applications of ship analysis. Class I coefficients seem to be the rule then, in addition to the fact that there is not, as of yet a program to extract the poles and their Class II coupling coefficients from the transient response. Class II coefficients should be used, or some amendments to the results must be added when the problem is a very large structure illuminated such that the transit time is long compared to fractions of a period of the dominant resonances. Such a case is the illumination of a ship when the incident wave is propagating from the stern to the bow, or vice versa. Then in the presence of two masts on the ship, there would be two distinct sets of poles and their residues, that are being excited at different times.

In equation (3.01) the exponential of $(s-s_i)$ should, for the general case be $-m_i$, as opposed to -1, denoting the multiplicity of the i^{th} pole. It has been determined though, that in scattering problems for spheres, there are only simple poles, and it is conjectured that the same is true for all other finite sized objects as well, since there has not been any evidence to the contrary[28]. Multiple poles have been shown to exist in some problems, such as poles in the exciting source - a ramp[17] with a double pole at the origin, and with resistively loaded antennas, such that they are critically damped, as found by Tesche[29]. Even so, Van Blaricum[17] extended Prony's method to include the calculation of any multiple poles.

3.2 SEMPEX CODE METHODS

Lager, Hudson, and Poggio[30] developed a computer code, SEMPEX, based on Prony's method for the Air Force Weapons Laboratory's CDC 7600. This program neglects the entire function, assumes simple poles and class I coupling coefficients. The program was acquired and implemented on NSWC's CDC 6500. Implementation required a bit of debugging to eliminate some errors such as complex multiplication of very large numbers and division by zero. In addition a change was made in the calculation of Δt which took into account the beginning time of the digitized waveform. Figure 3.1 presents the flowchart of the program with appropriate numbers denoting the equations in the Chapter 2 derivation of Prony's method.

The input data for the program are 512 equally spaced data samples of a response waveform. This is presumably for compatibility with a Tektronix 7912 digitizer. The mean of the waveform is calculated and subtracted from each sampled value. This apparently is not a required step, and in fact causes some confusing results,

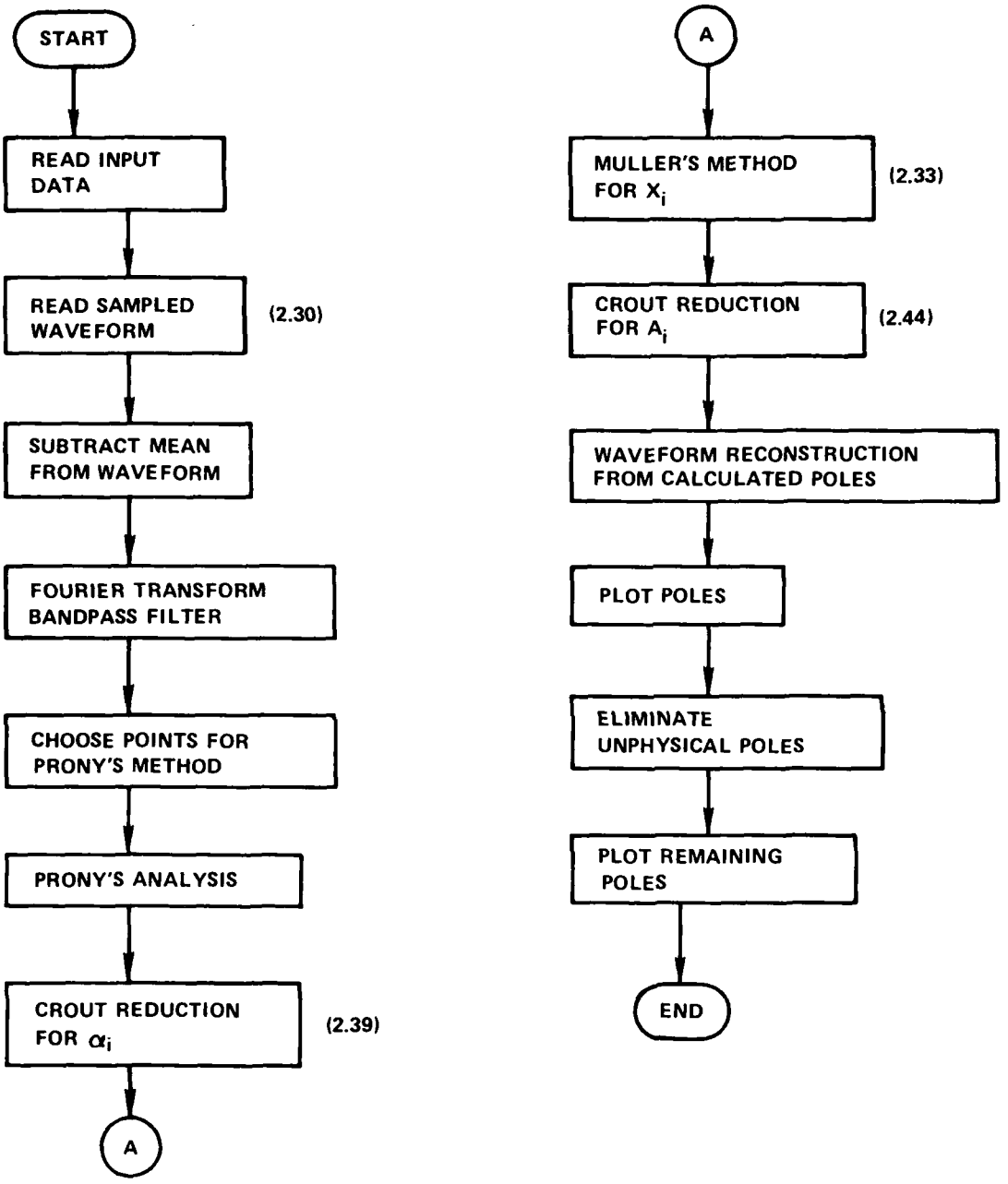

FIG. 3.1 SEMPEX FLOWCHART

(errors), if one is not aware of its presence. The original intent of this operation was to correct for drift in some oscilloscopes on a transient range. The waveform is Fourier transformed and bandpass filtered at the user's option, between chosen frequencies. The bandpass filter is a perfect one, such that energy in frequencies outside the pass band is identically zero. It must be remembered at this point that the poles of the filter are introduced here. With an inverse transformation, a waveform is retrieved, and of the original 512 points only a few are used for the Prony analysis subject to several constraints to be explained later. In the case that M > 2N in equation (2.30), then the least square method is used to transform the matrix A of equations (2.39 and 2.40A) to a square one. Thus in equation (2.39)

$$[A]\ [B] = C \tag{3.2}$$

it is necessary to solve for the coefficients α_i in vector B to minimize

$$\Phi = \sum_{i=1}^{N} r_i^2 \tag{3.3}$$

where

$$r = F\ C - B \tag{3.4}$$

the vector of residuals. The minimum occurs at that point when all the partial derivatives with respect to the coefficients α_i are zero. Thus, we are looking for the vector B such that

$$\nabla\Phi = 0 \tag{3.5}$$

where

$$\nabla = \frac{\partial}{\partial\alpha_1}, \frac{\partial}{\partial\alpha_2}, \frac{\partial}{\partial\alpha_3}, \ \ldots\ \frac{\partial}{\partial\alpha_N} \tag{3.6}$$

Then these are the forms of the "normal equations of least square", where now

$$A^T\ A\ B = A^T\ C$$

is solved for vector B, and the A^T A matrix is square. This matrix equation is solved by the Crout reduction method[31]. The roots of the polynomial equation (2.33) are found by Muller's method. The residues are calculated by equation (2.44), by again employing the Crout reduction technique. The calculated poles and the residues are now plotted and are used to construct a waveform for the comparison with the original response. Then, if selected, the user has the option to eliminate poles which are obviously not physical, and again recalculate the response for the comparison.

3.3 SEMPEX INPUT PARAMETERS

The user must provide the following data, as shown in Table 3.1.

RESPIN - the array that contains the original 512 sampled data points.

NPOLES - is the number of poles that are to be extracted from the function. If the number of poles is known, NPOLES should be chosen to be two to four more, to allow a better fit of the data, and to provide a check on the actual number of poles. The extraneous poles should have very small residues and, therefore, be easily identifiable. When the number of poles is unknown, the procedure as stated in the instructions is to ask for as many poles as possible and then to observe the results. When far too many poles have been requested the matrix A in equation (3.7) will become singular and the program will exit. In such a case the number of requested poles should be reduced for each run, and the poles with the large residues, due to the resonating structures, should remain stationary, while the "curve fit" poles will experience a great deal of movement in the s-plane.

NBEGN - is the index number (1 - 512) of the first data point to be used in the analysis. NBEGN should be chosen such that it is after the time that the driving function has decayed or gone to zero. This especially must be the case if the driving function cannot be expressed as a sum of complex exponentials[17]. At times, the driving function such as the Guassian pulse, which cannot be expressed as a sum of damped exponentials and does not decay to zero until infinity, the excitation function must be deconvolved from the response function. When the exciting function can be expressed as a sum, and does not fall to zero quickly, then the poles of the exciting function will also appear in the output poles in the s-plane.

NDECI - determines the sampling interval for the points that are chosen for the Prony analysis. Figure 3.2 illustrates a typically sampled waveform. NDECI must be small enough to avoid pole foldover, analogous in aliasing in the discrete Fourier transform. It must satisfy the Nyquist criterion.

$$\text{NDECI} \leq \frac{\Delta t}{2 f_{max}} \tag{3.8}$$

where

Δt = the spacing between the original data points

f_{max} = the highest frequency component in the waveform

Table 3.1. SEMPEX Input Data

Parameters for Prony's Method	Parameters for Calculated Pole Manipulation
RESPIN	RES
NPOLES	RHP
NBEGN	PREAL
NPTS	PIMAG
NDECI	
FLOW	
FHIGH	

NTPS - is the number of points that Prony's method will work on. One constraint is that

$$\text{NPTS} \geq 2\ \text{NPOLES} \tag{3.9}$$

this is equivalent to the statement $M \geq 2$ NPOLES gives an exact system, such that matrix A in equation (3.2) is square. For $M > 2$ N, the least square method is employed. Another constraint on NPTS is that the index of the last point must be less than 512.

$$\text{NPTS} \leq \frac{512 - \text{NBEGN}}{\text{NDECI}} + 1 \tag{3.10}$$

FLOW - specifies the low frequency cutoff of the perfect bandpass filter.

FHIGH - specifies the high frequency cutoff of the perfect bandpass filter. To avoid distortion of the retrieved waveform, the inverse Fourier transformed filtered spectrum, due to windowing, the bandpass filter must be chosen carefully such that FLOW and FHIGH occur in deep notches of the original spectrum, that are at least two orders of magnitude below the peak[32].

The following parameters are only used to eliminate the possible nonphysical poles from the set that are extracted by the Prony technique. Figure 3.3 shows the location of PREAL, PIMAG, and RHP. RES is used to eliminate poles that decay too fast.

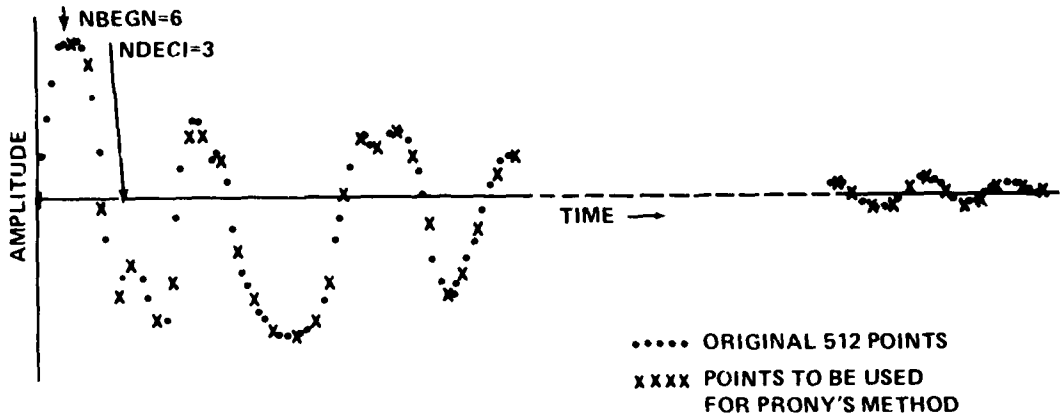

FIG. 3.2 DEFINING A WAVEFORM FOR SEMPEX

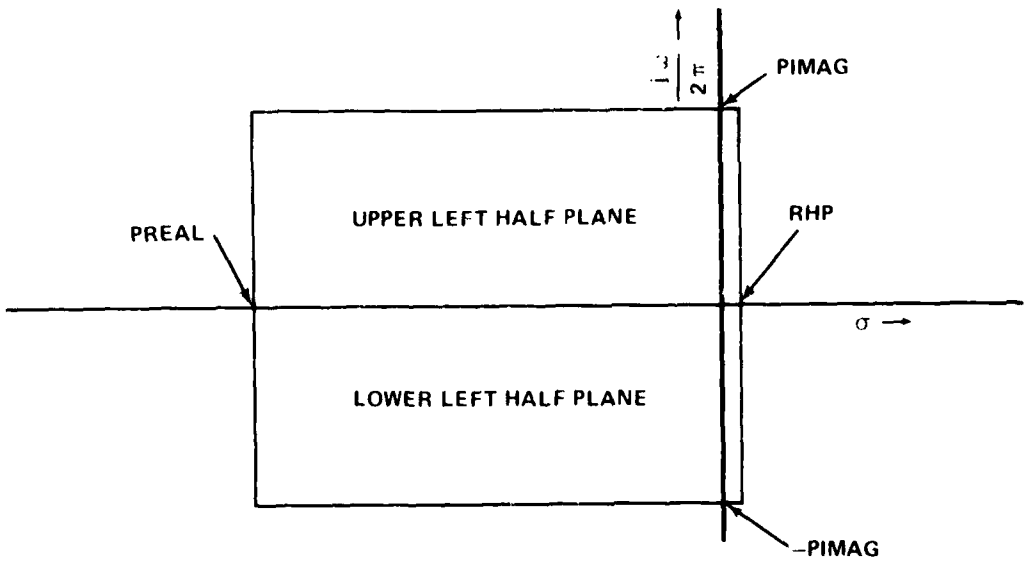

FIG. 3.3 DEFINING S-PLANE FOR PHYSICAL POLE LOCATION

CHAPTER 4

EXPERIMENTAL FIELD WORK

4.1 THE EMPRESS FACILITY

The Naval Surface Weapons Center operates a test facility for EMP related experiments in Solomons, Maryland, designed and built by IITRI. The facility, EMPRESS (EMP Radiation Environment Simulator for Ships) is located near the mouth of the Patuxent River, such that the test site could be accessible by destroyer class ships. The EMPRESS Facility provides a subthreat level environment for analysis of shipboard EMP response and coupling. The facility consists of a pulse generator, and a top loaded conical antenna.

The pulse generator is a 2.5 MW peaking capacitor source (PULSPAK 8000), designed and built by Pulsar Associates, Inc., and it operates in the vertical mode as a monoconic pulser. It uses a 50 stage high inductance Marx generator and each stage can be charged to as much as 50 kV, and has a total output capacitance of 4 nF and a maximum stored energy of 12 kJ. Because of the "high" Marx inductance distributed peaking capacitors are used to obtain a risetime of 10 nanoseconds.

Figure 4.1 shows EMPRESS; the Marx generator, peaking capacitors, umbilical cord for remote control and the bottom of the 30° conical antenna.

With the closing of the main spark gap in the pulser, a pulse is fired into the 28 meter tall conical antenna, which, in the early time looks like an impedance of 75Ω, to radiate the vertically polarized fields. To prevent and/or delay reflections that would degrade the EMP simulation, the antenna is top loaded by a cylindrical transmission line that is 380 meters long and is terminated in 300Ω to ground.

The layout of EMPRESS with respect to the "interaction area" is pictured in Figure 4.2. The field in and around the interaction area has been well documented[55] and some relevant excerpts appear in Appendix B. Figures 4.3 and 4.4 show a sample EMP electric field and its Fourier transform. The spectrum is fairly constant to 1 MHz, then drops off at about 18 dB/decade to 20 MHz and then 26 dB/decade through 100 MHz. Thus, frequencies above 70 MHz are down by at least

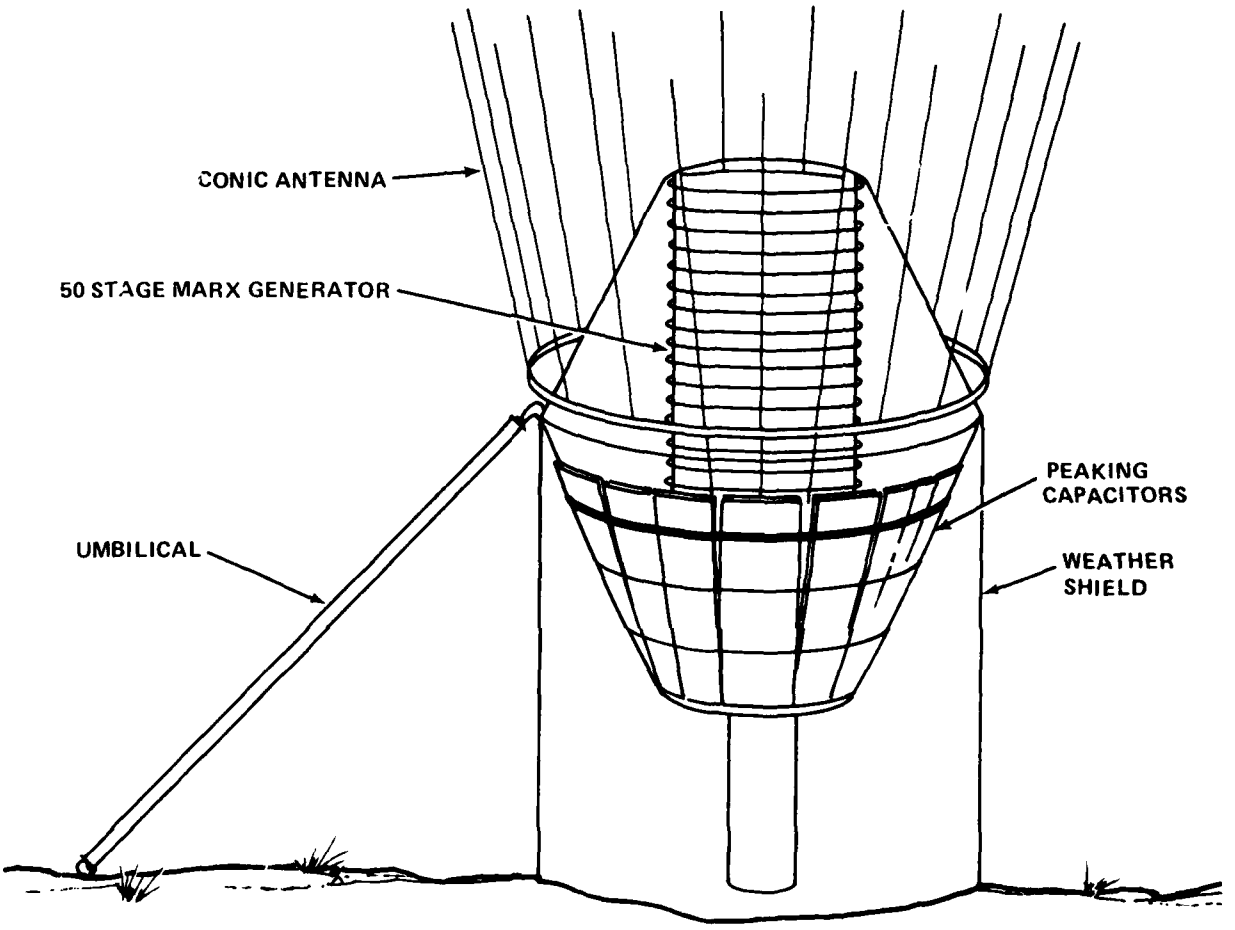

FIG. 4.1 EMPRESS

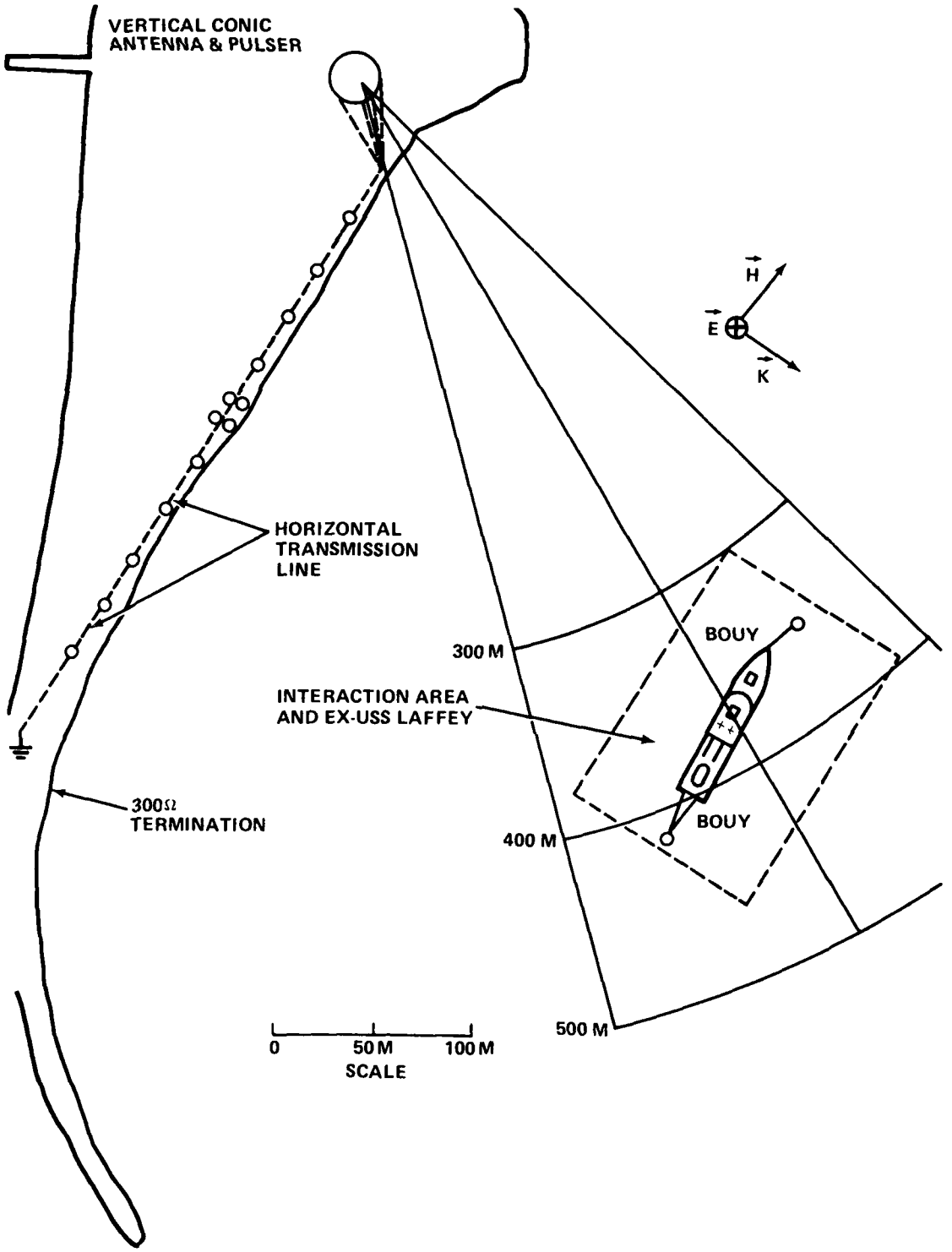

FIG. 4.2 NSWC FIELD TEST FACILITY, SOLOMONS, MD

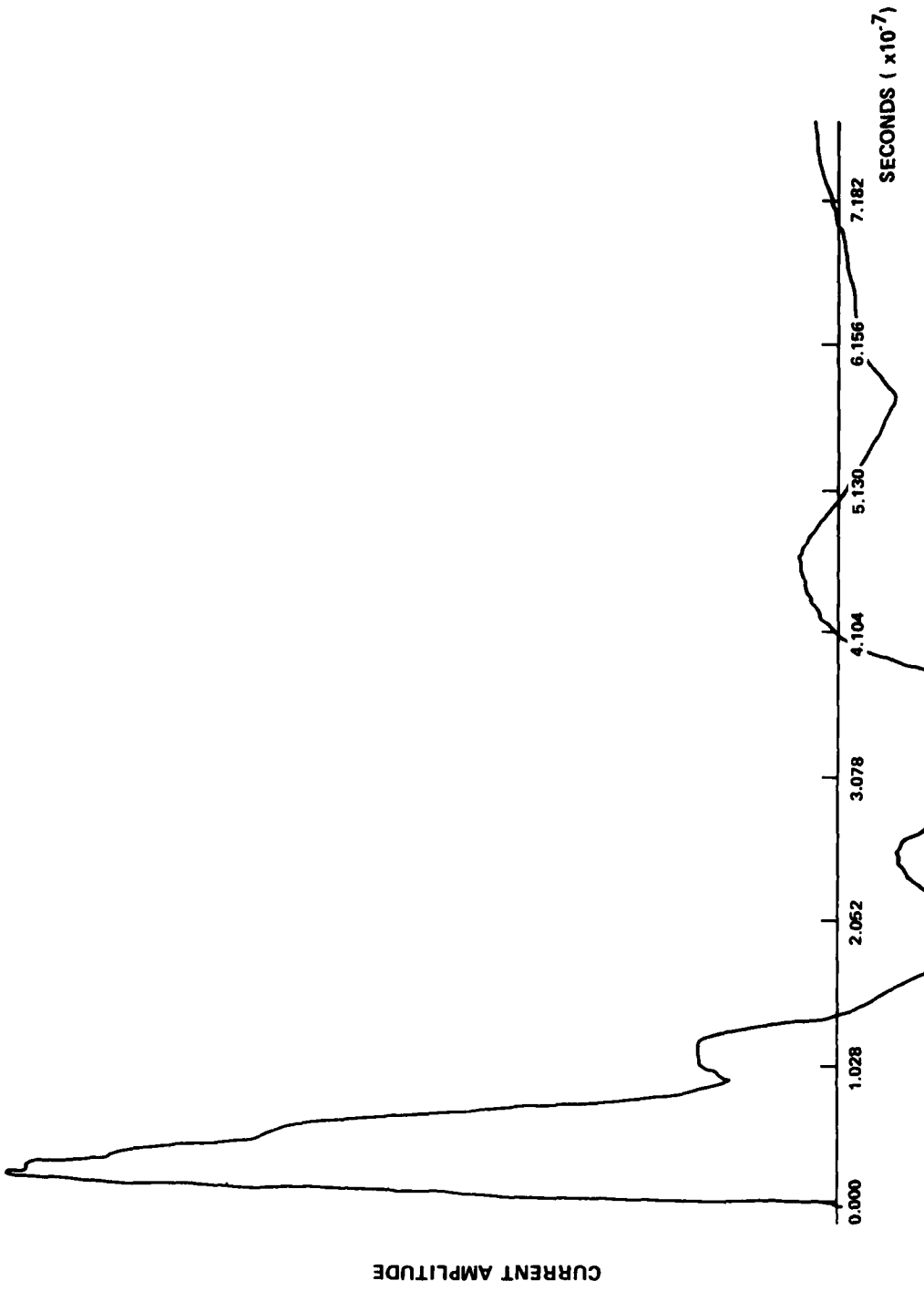

FIG. 4.3 EMPRESS ELECTRIC FIELD WAVEFORM

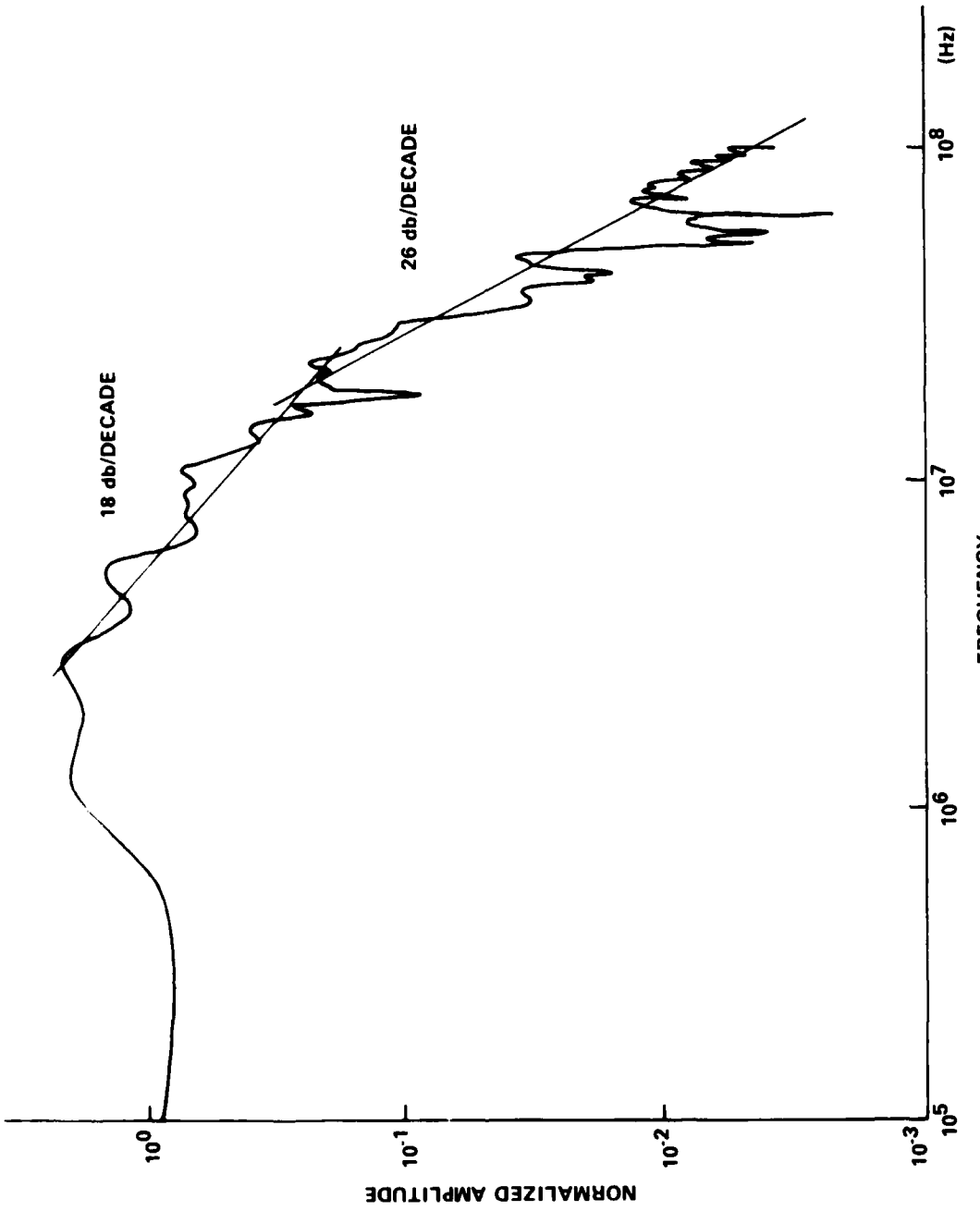

FIG. 4.4 EMPRESS ELECTRIC FIELD FOURIER TRANSFORM

two orders of magnitude. The amplitude at the anchorage point is 2.7 kV/meter providing an environment for subthreat level experimentation. The EMP simulating field is a propagating plane wave at the ship and the peak magnetic field is 2,700/377 A/meter, or 7.2 A/m.

The test vessel, on which all experiments were conducted, is the recently decommissioned USS LAFFEY. The LAFFEY is a DD class destroyer, with three five inch guns and MK 46 torpedoes. Though decommissioned, all electronic gear is still on board for EMP coupling tests. Since the ship is only recently inactive, all electrical connections are still good, and have not yet been affected by adverse weather and salt.

4.2 TEST EQUIPMENT

During the EMP coupling experiments at NSWC, a system for data acquisition has been developed. It consists of isolated test equipment with which it is possible to get hard copy pictures of any transient response. Data that have been recorded in the course of EMP work are: transient electric and magnetic fields, skin currents, bulk cable currents, and a variety of current and voltage measurements at antenna and electronic equipment terminals. For this experiment, the measurements are transient short circuit currents at the bases of antennas and ends of cables. The main instrument in such a test "setup" is a Tektronix 454A oscilloscope operating in the single sweep mode. The 454A's bandwidth of 150 MHz well exceeds the 70 MHz bandwidth of the EMPRESS Facility. Data is recorded from the face of the oscilloscope using a Polaroid Type 32 oscilloscope camera. The transient response is input to the oscilloscope via a test cable which can be connected to a variety of sensors and probes. The waveforms recorded on Polaroid film are brought back to NSWC laboratories for different types of analyses and cataloging[34]. Previously the main interest was the peak amplitudes of waveforms for determination of threshold levels for upsets, but now with Prony's method the complete waveform becomes very important and the pictures are fully utilized.

The scope naturally is subject to EMP upset and many precautions have been taken to reduce this possibility. With the ship at its anchorage point there are two types of power available - shore power and a diesel generator. Since transients can be induced on all cables, power lines included, neither of these power sources can be utilized. Power, therefore, is obtained from rechargeable 12V lead/acid automotive batteries. A fully charged battery can operate a 454A for almost 12 hours. 12 VDC is converted with a 300 W inverter and upsets due to power line transients are thus eliminated. Protection against electromagnetic fields in the testing environment is also required. It has been found that the operation of an oscilloscope in a high amplitude electromagnetic transient field will seriously affect the resulting waveform. For this purpose each oscilloscope is shielded by a metal box - "scope box". The scope box is made from aluminum, for ease of handling, and is just

large enough to contain the oscilloscope, the power inverter, and the camera. The battery is situated outside the scope box in another aluminum box, and battery power is transmitted to the inverter via a shielded umbilical cable.

The scope box is equipped with feed-through connectors for shielded connections between incoming signals on RG 214 or RG 58/U coaxial cables and short cables that connect to the scope. The test cable usually used, is double shielded coaxial RG 214. It has been found that in high field areas, such as near the mast, even with as much as twenty feet of cable no appreciable coupling can be detected into the test cable itself.

In this test of antenna currents, the test cable was connected to a current probe (Singer 91550-2), i.e. "Dash-2". Data on the current probe are shown in Table 4.1. The Dash 2 probe can be clamped around a cable to measure current, or a shorted loop to measure magnetic field, with appropriate calibration factors. The basic data acquisition setup is shown in Figure 4.5.

In actual EMP experimentation, problems with triggering the scope have shown up, and the process of obtaining a complete sweep on the oscilloscope, including a short presweep to guarantee the beginning of the waveform is quite an art. It has been found that external triggering using a short piece of RG 58/U attached over a ground plane, the scope box, works well for setups on deck. Within the ship though, another Dash 2 can be connected to a cable, which is known to carry high amplitude current, to externally trigger the 454A.

The measurement of short circuit current, I_{sc}, was accomplished by making a small adapter that would short the inner conductor to the outer in a loop just big enough to accommodate the Dash 2 probe. The I_{sc} adapter was made small so that there would be little or no magnetic field coupling through the loop. The adapter fits onto a connector at the base of the antenna, and is also used at the cable end measurements inside the ship, at the radio equipment.

4.3 PRELIMINARY SHIPBOARD WORK

As mentioned in the introduction, one motivation for the study of pole extraction at NSWC, was to identify and analyze shipboard resonant structures with respect to antenna location. For this experiment, two identical antennas on the ex-USS LAFFEY were chosen, as each was located in radically different environments on the ship. In addition there was interest in them, since in a previous ship test it was discovered that the short circuit current at the base contained relatively high amplitude currents in the 2-15 MHz range, much below the pass band of the antenna, 250-400 MHz. One of the antennas is on top of a gun mount in the forward part of the deck, and the other is on the top of the mast. The two antennas also

Table 4.1. The Dash 2 Probe

Parameter	Singer 91550-2
Frequency Range	10 KHz - 100 MHz
Transfer Impedance	1.0 Ω
RF Current Range	0 - 100 amps
Max Power Current	350 amps (60 Hz)
Max Power Voltage	No limit; subject to adequate conductor insulation
Output Load Impedance	50 + j0 Ω
Sensitivity	10 ma = 10 mv, across 50 Ω
Output Connector	Type N
Window Size	32 mm diameter
Dimensions	90 mm long x 74 mm wide x 36 mm thick
Signal Cable Length	No limit; subject to cable frequency response

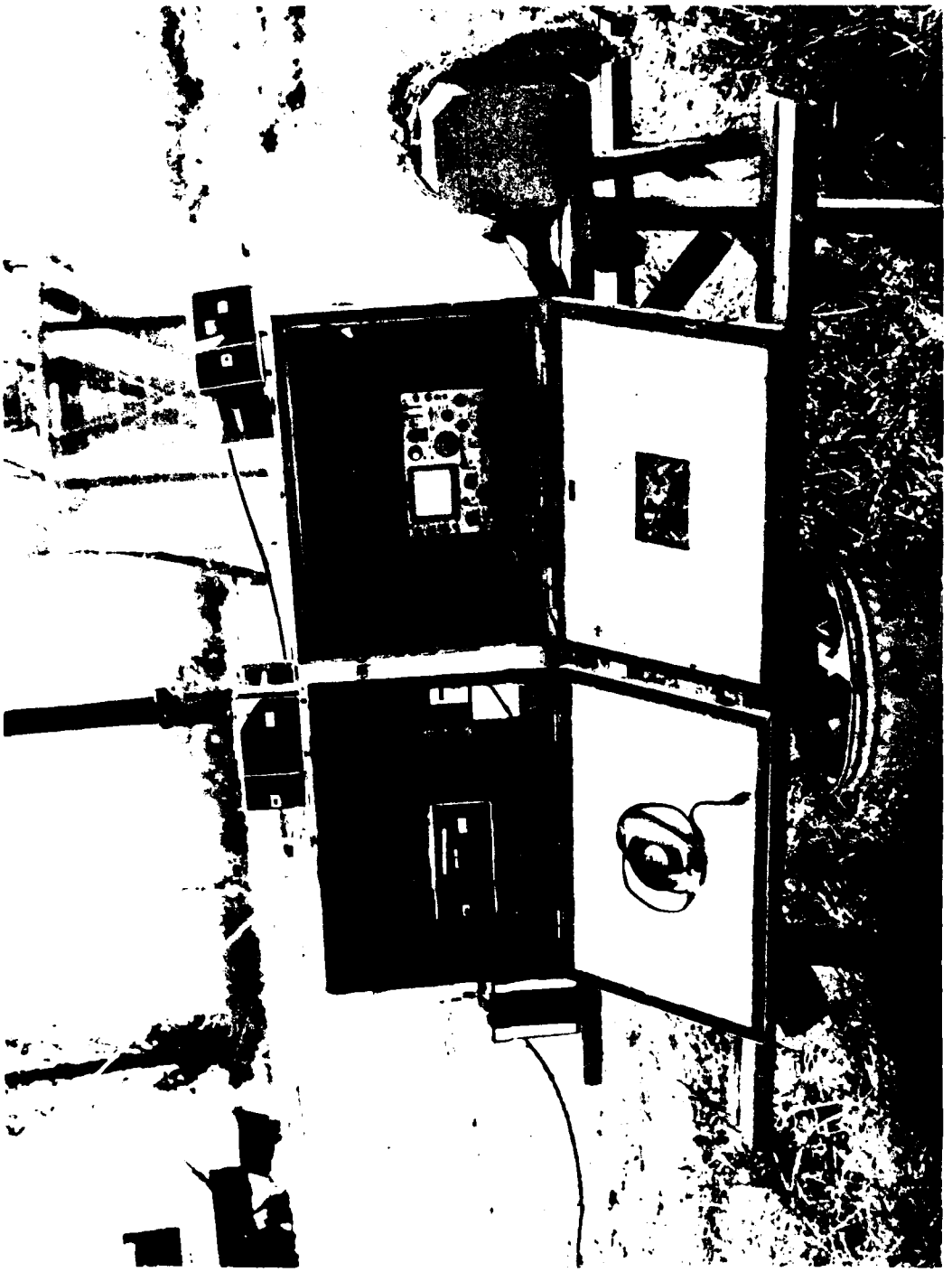

FIG. 4.5 DATA ACQUISITION SETUP

have radically different cable routings. For the mast antenna, the cable drops directly down alongside the mast and then down two decks to the Combat Information Center, the CIC. The cable from the gun mount antenna runs down through the gun mount, up and down several decks in the interior of the ship, then along a wall on the outside and finally ending up in the Radio Transmitter Room.

The experiment was to provide for Prony analysis, open circuit voltage (V_{oc}) and short circuit current (I_{sc}) waveforms, from both at the base of the antennas, and the ends of the cables at the equipment in their respective rooms. Poles from this analysis would be useful in the design of full-threat injection sources at the equipment's input terminal, provide knowledge of the effect of cable routing on the response waveform, and identify the resonating structures and to what degree they contribute to the response of the two antennas. Preliminary experimentation at the NSWC EMP Facility, showed extremely complicated waveforms, which were difficult to digitize. At this point it was determined that to increase the accuracy in digitization and to not overlook the finer aspects of the waveform, it would be necessary to use the delay time multiplier feature on the Tektronix 454A. The delay-time multiplier makes it possible to get a 2 microsecond waveform on a horizontal scale of 20 ns/cm. Figure 4.6 is a picture of a 20 ns/cm waveform and shows the first 200 ns of the waveform. The delay-time multiplier makes the screen of the oscilloscope look like a 200 ns window. This window is moved from one end of the waveform to the other, with pictures taken at each window position which overlaps the previous picture by a half, so that there is a complete set of pictures, which when merged together will show a 2 microsecond waveform. Figure 4.7 shows part of the merged waveform and the separate pictures through the 200 ns window, that combine for the complete waveform. Each picture of the waveform was literally cut up and pieced together, by hand and then by computer for the Prony analysis.

The complexity of the waveform required the windowing of the waveform and the piecing together of the results. This proved to be a difficult task. First of all, the waveforms are not identical from one picture to another, in the same window. This could be due to a number of reasons. One is that the location of the ship can change by as much as thirty degrees due to wind and tides, etc. In piecing together the waveform, it was usually almost impossible to match peaks, and the matching process degenerated into a guessing game providing a mostly useless waveform. Initially it was hoped that the discontinuities at the match points and the differences especially in the higher frequency components, would only introduce a small perturbation into the problem, but since Prony's method is very noise sensitive[17], this was not the case. To make an experimental procedure like this work, it is absolutely necessary for the waveform to be identical from EMP shot to EMP shot, especially when dealing with such a touchy problem as scattered fields to begin with. The complexity of the waveform

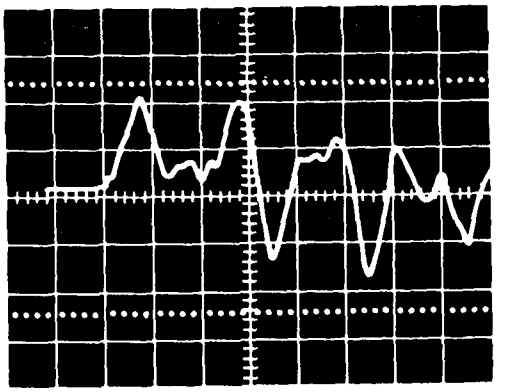

VERTICAL - 20 MV/CM

HORIZONTAL - 20 NS/CM

FIRST PART OF THE WAVEFORM

FIG. 4.6 A 20 NS/CM WAVEFORM

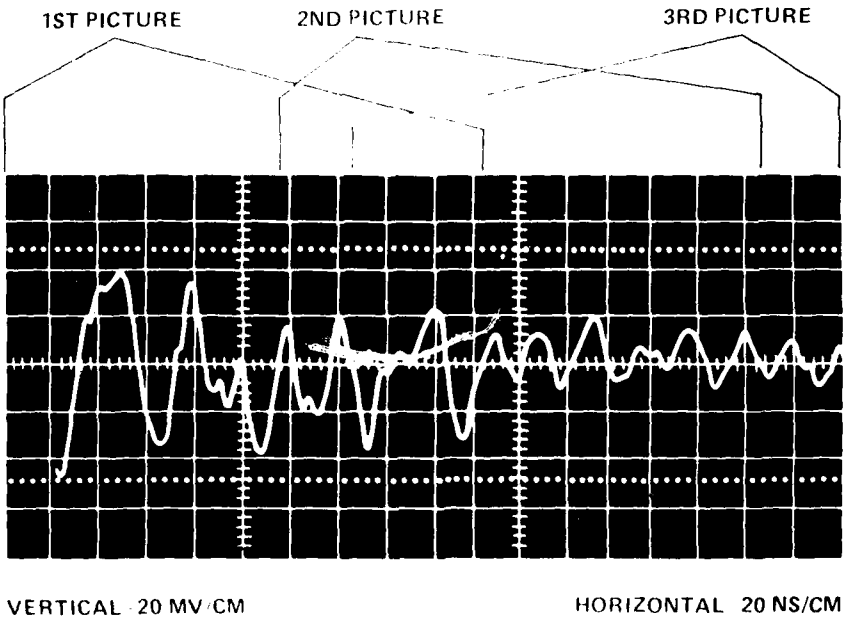

VERTICAL - 20 MV/CM

HORIZONTAL 20 NS/CM

FIG. 4.7 WAVEFORM MERGING

quickly brought to the surface another problem. How many poles could make up such a waveform, and how many poles are there in the scattered field from such a complex object as the superstructure of a ship anyway? The Prony's method program, in its present state, occupying almost 150 K of core for the extraction of 35 poles could not be expanded any more. And it is a fact that the scatter from a ship would include more than 17 pole pairs. In addition, because the use of the Prony method had not yet withstood a rigorous test of analyzing real experimental waveforms, it became clear that the program could not handle a waveform this noisy or complex.

4.4 FIELD WORK ON SHORE

The resulting decision was to put aside the problem of scatter from a ship, and begin to concentrate on the use of Prony's method on experimental waveforms. One of the antennas was removed from the gun mount and brought ashore, where it was erected on top of a shack 50 meters from the pulser. Here various scattering tests could be performed with the antenna as a receiver, and could hopefully provide cleaner and simpler waveforms. The antenna was retained for this experiment, because of the remaining interest in the analysis of its EMP response.

Metal objects in and around the area of the pulser were removed as much as possible such that the scattered field from an extraneous object would only reach the site of the shack about 200 ns after the EMP was first incident on the antenna. In addition, this extraneous scattered field would also be much lower in amplitude, due to the sizes of the extraneous objects, and the inverse dependence on r^2 of the scattered field. The only large structure available for use in this test was a 5 m by 1.5 m (dia) sewer pipe. Unfortunately the lowest resonance of the pipe was a bit too high, on the order of 30 MHz, a bit above the 2-20 MHz frequencies that are usually recorded in field tests. Testing included the recording of pictures of the short circuit current waveforms of the antenna, without the cylinder in the field. The experiment required the gradual moving in of the cylinder toward the antenna to see the change in waveform as the scattering object was brought closer and closer. The cylinder was finally put on top of the shack next to the antenna and then, even such that the antenna was on the shadow side of the cylinder. From the waveforms it seemed that the scattered field from the cylinder was having no effect on the response of the antenna, until it was placed very near the antenna. This is due to the low amount of energy in the dominant frequency range of the antenna response in the scattered field. Four sets of data were chosen for the Prony analysis. The first set was the EMP electric field waveform, recorded in the clear field, in the exact location where the antenna was placed. The second set was the AS-1018 response to EMP, where the antenna was mounted on top of the shack, and the short circuit current was recorded at the base. The third set was the I_{sc} response

of the antenna with the cylinder next to it on top of the shack; and the fourth was the I_{sc} response with the cylinder placed such that the antenna was on the shadow side. Figure 4.8 illustrates the various conditions of each test. The results of the analysis of the four test waveforms are listed in Appendix C.

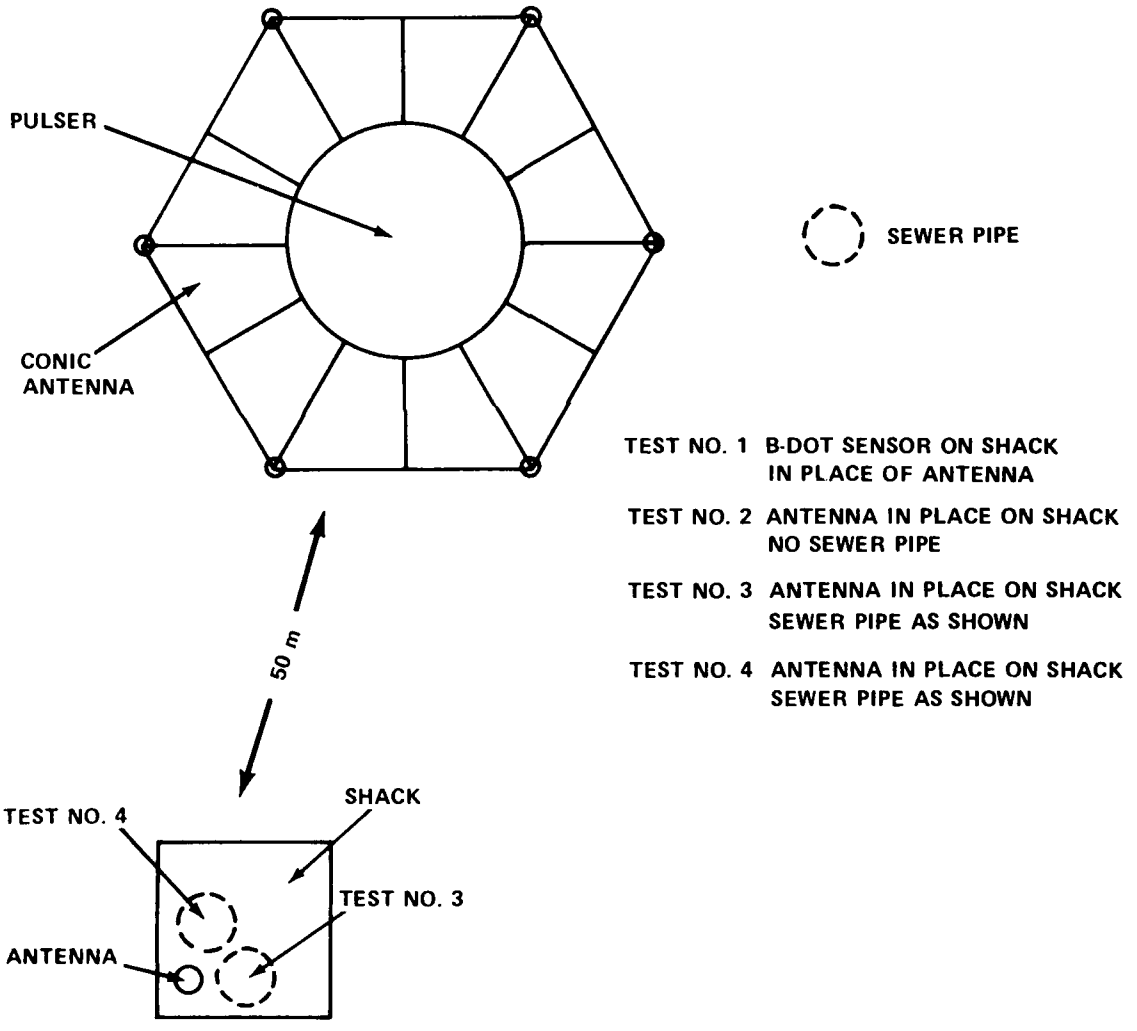

FIG. 4.8 FOUR FIELD EXPERIMENTS

CHAPTER 5

NUMERICAL ANALYSIS

5.1 DIGITIZATION AND THE TEST WAVEFORM

The analysis process begins with the digitization of the waveform. A Tektronix Graph Tablet was used in conjunction with a Tektronix storage graphics terminal. The terminal is part of the NSWC CDC 6500 timesharing system. The software for the terminal allows for the manipulation of the waveform in almost any possible way: merging waveforms, deleting sections, adding sections, Fourier transform, etc. SEMPEX though, currently demands that the waveform be in the form of 512 equally spaced data samples. A program was written to perform this transformation, also allowing for the option of "fitting" the original digitized waveform with line segments, or a cubic spline. The new "fit" curve was sampled at the 512 equally spaced points of time ranging over the entire waveform. The cubic spline was mainly used, because it provided smoother waveforms - possibly less noisy ones, concurrently. The line fit routine was more useful on the more complicated waveforms, when the cubic routine sometimes had the tendency to let the fit curve wander away from the real curve.

A test of the SEMPEX routine was performed by generating a function from five pole pairs, as shown in Figure 5.1, and then attempting to extract them.

$$
\begin{aligned}
f(t) = {} & .5\, e^{-10^{+6}t} \sin(2\pi 7\times 10^{6} t) + \\
& .5\, e^{-1.3\times 10^{+6}t} \sin(2\pi 10^{7} t) + \\
& .74\, e^{-4\times 10^{+6}t} \sin(2\pi 1.5\times 10^{7} t) + \\
& .65\, e^{-10^{+6}t} \sin(2\pi 2.4\times 10^{7} t) + \\
& .44\, e^{-8\times 10^{+6}t} \sin(2\pi 2\times 10^{7} t) \qquad (5.1)
\end{aligned}
$$

The waveform was bandpass filtered between two typical frequencies (2-35 MHz), as would be done for an experimental waveform. The results were surprising, in that the runs requesting, ten and twelve

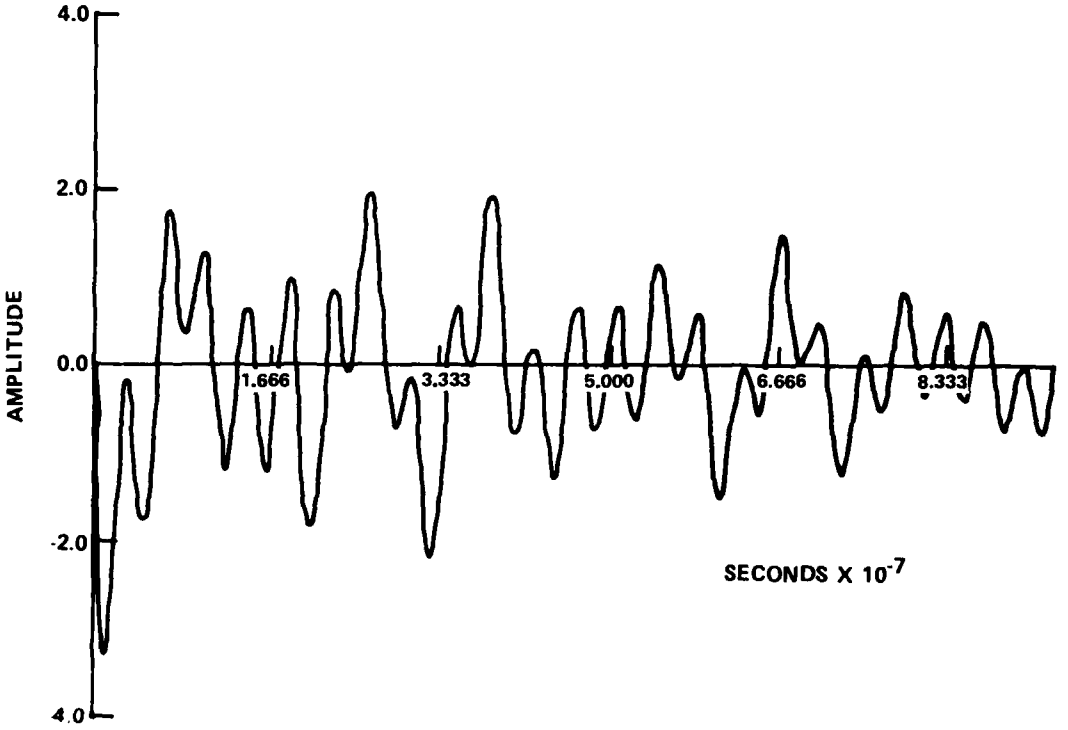

FIG. 5.1 TEST WAVEFORM

poles (NPOLES = 10, 12), the extracted poles were not even close to the input ones. When requesting 14 poles, the input poles were retrieved within a few percent error. Asking for more poles simply showed a lot of shifting in the residue value of each pole pair, and some shifting in the pole locations. It seemed clear that the Prony technique would be useless, if for a perfect waveform from ten poles input, the exact ten poles could not be extracted. The results from experimental waveforms could then be expected to be incomprehensible. It was at this point that the "mean subtraction" problem was realized, and the bandpass filter was thrown out. Subtraction of the mean from the waveform (see 3.2) caused very low frequency poles to appear, that originally had nothing to do with the waveform.

The bandpass filter was removed for several reasons. The filter itself has poles, and these are introduced into the waveform at the filtering stage; this complication of the problem is not needed. Further, the Fourier transformation introduces noise, and the inverse transformation does not remove it, but only increases it. The effect of noise in a waveform, is well documented by previous authors and, has been determined to be catastrophic. Noise must be on the order of 1-5% of peak or 35 dB signal to noise, in order for the Prony technique to extract quickly recognizable poles. Some have tried changing the filter, by giving it different roll-offs, but to no avail.

The test waveform was run again after the elimination of the mean and the filter. The result is shown in Table 5.1. Ten poles were requested, and the same ten poles were returned, exactly, with very small error in the reconstructed waveform. A run was made requesting the full 35 poles to be extracted; the result is shown in Table 5.2. The ten real poles were extracted, and 25 curve fit poles are all at least four orders of magnitude below the largest.

The least square method was adopted for all waveforms. Though guaranteeing the presence of curve fit poles, it provides Prony's method a little "more room to work with." In this stroke, the problem now becomes the process of finding the best curve fit poles and then hoping to identify the physical poles, as opposed to searching for the physical poles of which there is no conception of number, location, or magnitude of residue.

The waveform that was anlyzed first was that of the I_{sc} response of the antenna in the clear field. An initial set of runs showed that all the poles, not only the ones with the small residues showed considerable movement in the s-plane from run to run, such that the hope of identifying the real poles of the system were lost (see Table 5.3). Upon examining the input parameters and the resulting poles, a method that not only finds the best fit poles for the waveform but also eliminates many pole groupings that had been considered correct in previous analyses was constructed.

Table 5.1. Test Waveform Without Filter

	Magnitude of Residue (ampl)	Real Part of Pole Location (nepers)	Imaginary Part of Pole Location (Hz)
1.	.49902E+00	-.99805E+06	.69863E+07
2.	.49902E+00	-.99805E+06	-.69863E+07
3.	.49873E+00	-.12975E+07	.99805E+07
4.	.49873E+00	-.12975E+07	-.99805E+07
5.	.74416E-01	-.39922E+07	.14971E+08
6.	.74416E-01	-.39922E+07	-.14971E+08
7.	.43810E+00	-.79844E+07	.19961E+08
8.	.43810E+00	-.79844E+07	-.19961E+08
9.	.64873E+00	-.99804E+06	.24951E+08
10.	.64873E+00	-.99804E+06	-.24951E+08

NPOLES = 10
NBEGN = 2
NPTS = 40

NDECI = 10
F2NYQ = 25.55 MHz
RMS ERROR = 7.57×10^{-6}%

Table 5.2. Test Waveform Requesting 34 Poles

	Magnitude of Residue (ampl)	Real Part of Pole Location (nepers)	Imaginary Part of Pole Location (Hz)
1.	.52265E-06	-.11192E+08	.13740E-10
2.	.10337E-19	.29781E+08	-.32506E-09
3.	.30214E-06	-.73795E+07	.74302E-07
4.	.16201E-06	-.74207E+07	.67890E+07
5.	.16177E-06	-.74207E+07	-.67890E+07
6.	.49902E+00	-.99805E+06	.69863E+07
7.	.49902E+00	-.99805E+06	-.69863E+07
8.	.49873E+00	-.12975E+07	.99805E+07
9.	.49873E+00	-.12975E+07	-.99805E+07
10.	.12305E-05	-.83308E+08	-.11403E+08
11.	.12305E-05	-.83308E+08	.11403E+08
12.	.74416E-01	-.39922E+07	-.14971E+08
13.	.74416E-01	-.39922E+07	.14971E+08
14.	.28055E-06	-.19563E+08	.16723E+08
15.	.28263E-06	-.19563E+08	-.16723E+08
16.	.43810E+00	-.79844E+07	.19961E+08
17.	.43810E+00	-.79844E+07	-.19961E+08
18.	.91430E-11	.76394E+07	.20344E+08
19.	.91523E-11	.76394E+07	-.20344E+08
20.	.64873E+00	-.99805E+06	.24951E+08
21.	.64873E+00	-.99805E+06	-.24951E+08
22.	.23851E-07	-.19129E+07	-.25585E+08
23.	.23924E-07	-.191293+07	.25585E+08
24.	.14472E-09	.34404E+07	-.29714E+08
25.	.14491E-09	.34404E+07	.29714E+08
26.	.47873E-09	.29847E+07	.33494E+08
27.	.47891E-09	.29847E+07	-.33494E+08
28.	.10298E-07	-.70296E+07	.34713E+08
29.	.10348E-07	-.70296E+07	-.34713E+08
30.	.23154E-07	-.89421E+07	-.38494E+08
31.	.22950E-07	-.89421E+07	.38494E+08
32.	.14870E-11	.89367E+07	-.38911E+08
33.	.14867E-11	.89367E+07	.38911E+08
34.	.47071E-14	.12482E+08	-.42583E+08

NPOLES = 34
NBEGN = 2
NPTS = 84

NDECI = 6
F2NYQ = 42.58 MHz
RMS ERROR = 2.302×10^{-6} %

Table 5.3. Shifting Pole Locations

	Imaginary Part of Pole Location Run #1 (MHz)	Imaginary Part of Pole Location Run #2 (MHz)
1.	6.5663	4.5368
2.	12.946	7.7514
3.	13.071	12.751
4.	19.620	21.382
5.	28.379	28.671
6.	39.886	39.123
7.	43.463	43.972
8.	55.396	55.654
9.	67.526	66.651
10.	67.825	68.990
11.	79.491	83.343
12.	91.279	85.235
	NPOLES = 25 NBEGN = 1 NPTS = 84 NDECI = 6 F2NYQ = 91.2 MHz RMS ERROR = 4.48%	NPOLES = 24 NBEGN = 1 NPTS = 84 NDECI = 6 F2NYQ = 91.2 MHz RMS ERROR = 8.08%

5.2 FORMULATION OF THE NYQUIST CRITERION CONSTRAINT

The key to this constraint method is to sample the original 512 points in such a way that Prony's method is constrained to look for poles whose imaginary part (ω) will be below twice the Nyquist rate. This in general brings about two results. The first is psuedo-filtering. Instead of the noisy Fourier transformations and the perfect bandpass filter, by specifying the Nyquist frequency, the pole locations calculated will have to be below twice that frequency, thus providing a type of filtering. The other result is pole foldover. Ideally (computer generated cases) there can be an infinite number of poles for any structure in the impulse response. In an actual field case, the incident field's frequency spectrum is known, such that the effects of pole foldover, while existing, can be minimized by proper choice of an upper frequency. This frequency is defined such that, it is substantially above the dominant frequencies of the waveform, the imaginary part of the pole locations of the structure. Called F2NYQ, it is calculated by

$$F2NYQ = \frac{512}{NDECI\ 2\ TMAX} \tag{5.2}$$

where NDECI is the sampling interval for the points, and TMAX is the total duration of the sampled waveform. Of four input parameters (NDECI, NPOLES, NPTS, NBEGN), two (NPTS, NBEGN) are used to specify the size and position of the window, through which only part of the waveform is observed and analyzed. Using windowing makes it possible to look at several sections of a waveform and then to average the results, in an effort to try to find the real poles. The process of windowing is gaining popularity as a way of eliminating the curve-fit poles from the results. The basis for this is that, through windowing, the real poles of the system should not be subject to great deviations in location, from window to window, while the curve fit poles will, or at least should. Several types of windowing techniques are illustrated in Figure 5.2.

Specifying the number of poles is the final step in the constraint method. Prony's method is thus forced to look for NPOLES below a certain frequency, where there may be n poles in the real system. By observing the resulting calculated poles for a certain F2NYQ, for many NPOLES, one will soon notice a phenomenom already recorded by others[17,23,24]. This is the appearance of the right half plane (RHP) poles. These poles are known to be nonphysical, and therefore should be eliminated. The other poles calculated in that run should also be discarded since their residues and their pole locations are affected by the RHP poles. It is not correct to eliminate them and then recalculate the residues for the remaining poles.

A simple explanation of the phenomenon of the appearance of the RHP poles is as follows. Given: there are n poles in the physical

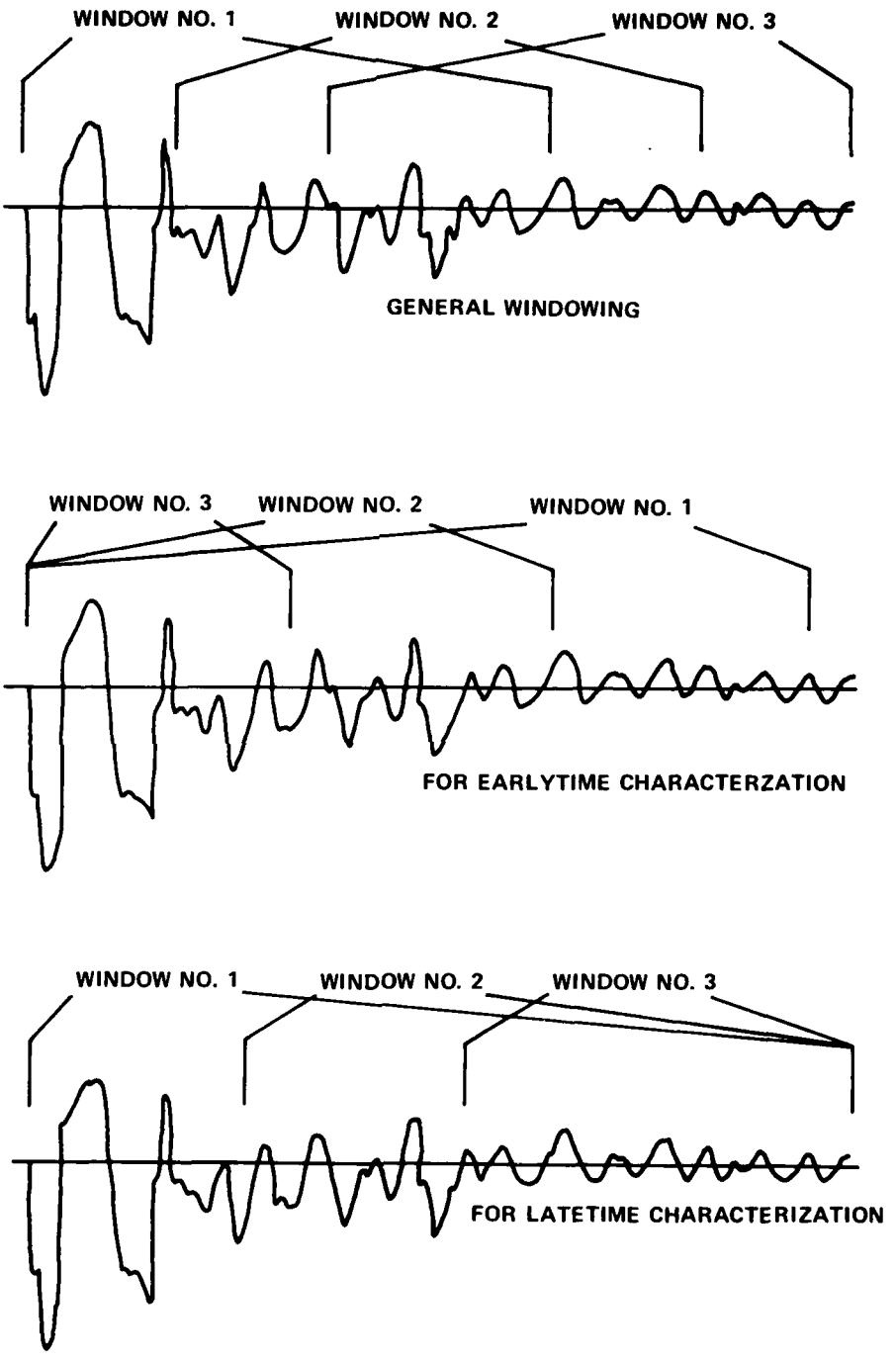

FIG. 5.2 WINDOWING TECHNIQUES

system below F2NYQ. If NPOLES < n is requested, one can expect large errors in the waveform that is reconstructed using these poles, since with fewer than n poles the waveform cannot be adequately described. As NPOLES → n, the errors should quickly become small, and when NPOLES gets bigger than n more curve fit poles are added to the results such that the fine structures of the digitized waveform can be described, thus slowly lowering the error of the reconstructed waveform with increasing NPOLES. Finally, when NPOLES > n, there is so much pressure on the Prony method that it begins to seek poles in the RHP to cancel the effects of the excess curve fit poles in the left half s-plane. Thus when right half plane poles appear, it is clear that there is too much pressure on the method for the given F2NYQ. This provides an upper limit for the possible number of poles in the bandwidth of F2NYQ. It may then be observed that if F2NYQ is raised sufficiently, the RHP poles will disappear. There are then three things to consider in the analysis of a waveform: the size and location of the windows, NPOLES, and F2NYQ.

Figure 5.3 illustrates the physical limits of the analysis process. The figure is drawn for a typical waveform encountered in EMP response work for ships. These are pictures of waveforms recorded on a scale of 50 ns/cm for a total size of .5 microseconds, for use with the currently available Prony's method program SEMPEX. The graph shows the possible F2NYQs plotted against the NPOLES that can be requested, and defines the boundaries, within which, the poles can be calculated. The rightmost boundary NPOLES = 35 is defined by the computer program. For a system containing more than 17 pole pairs it would be necessary to expand the program, thus moving the vertical boundary further to the right. This would require much more computer core than is currently used, which is 150K, half the capacity of the NSWC CDC 6500, and the full capacity for daytime use. The top boundary is not of interest, but it is subject to a constraint set of F2NYQ and NPTS (> 2 NPOLES) as discussed below. The left-most boundary is also immaterial for one can always specify NPOLES = 2, and there are few cases that contain only one pole pair in the data. The location of the lower boundary is of most interest. It is near this boundary line that most of the results are obtained. The boundary can be calculated by

$$\min \text{NPTS} = 2\ \text{NPOLES} + 2 \tag{5.3}$$

requiring a least square fit, and such that

$$\max \text{NDECI} = 512\ /\ \min \text{NPTS} \tag{5.4}$$

which provides for the analysis of the computer waveform of 512 points, and the boundary is then defined by

$$\min \text{F2NYQ} = \frac{512}{\max \text{NDECI}\ 2\ \text{TMAX}} \tag{5.5}$$

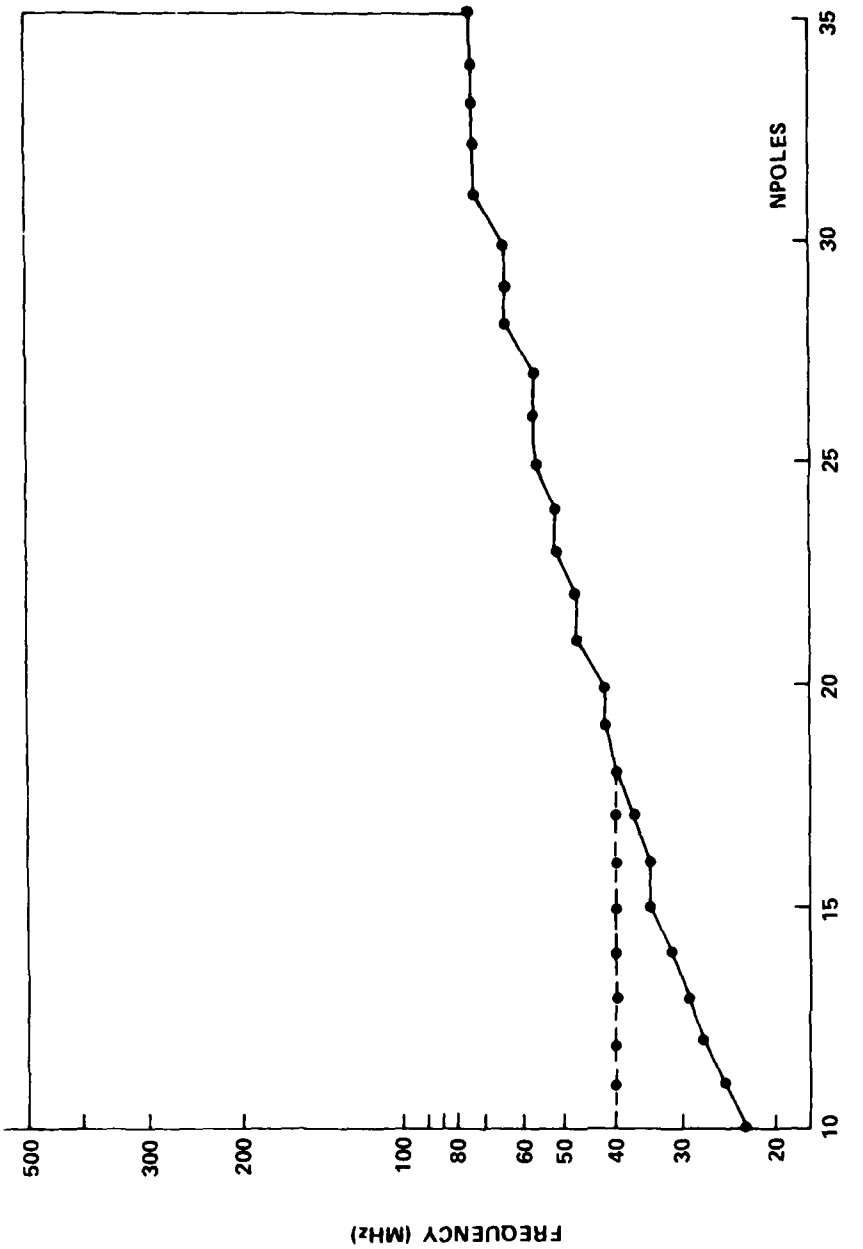

FIG. 5.3 LIMITS OF POLE CALCULATION ANALYSIS

It is not advisable to make runs using min NPTS, because the least square method is not given enough points to work with. It is generally better to have more points for practicality and a better fit to the data. Therefore, the boundary is only a theoretical one, and though results can be obtained on it, the practical boundary would be at a slightly higher F2NYQ for the same NPOLES. In the analysis proposed here, the method is to look at the results of specific F2NYQs by fixing NDECI and then moving left and right in the plane by varying NPOLES. There is also another limit as previously stated, that of pole foldover. For the purposes of ship EMP response the lowest F2NYQ that can be requested is on the order of 40 MHz (Figure 4.4), thus the dotted boundary in Figure 5.3.

The computation method is illustrated in Figure 5.4, in flow-chart form. Given a waveform the min F2NYQ is set by the practical physical characteristics of the system. The first run is made in the right hand bottom corner of the "allowable" section, Figure 5.5, point A. If no RHP poles appear then this means that not enough poles were forced into the band below F2NYQ. Then, it is necessary to lower F2NYQ, or to increase the number of poles to increase the pressure on the method. Since the run was made at the point with the maximum possible pressure, all that can be done is to make more runs following path I, Figure 5.5, down the bottom border left and down, to see if there were many high frequency curve fit poles, such that RHP poles may then appear. Such a case is illustrated in Table 5.4. Notice the large number of "high frequency" poles. If at point B still no RHP poles appear, then there are too many poles, including the curve fit poles, in the system for SEMPEX to extract. Many curve fit poles implies that the waveform is noisy either due to the original data, or the digitization process. If RHP poles do appear then path II, up and left, may be followed to lessen the pressure, until the point is reached where the RHP poles disappear again. If at point A, RHP poles appear, then too many poles for the F2NYQ were requested and either F2NYQ is raised or NPOLES is lowered, or both. This procedure of course can be started and used in any part of the plane, and eventually one will converge to a point where the RHP poles appear.

As can be seen there are many ways to find that border at which the RHP poles appear and it is known that the real pole locations can be found, Table 5.4. The use of this method will be illustrated in the following example on one of the waveforms taken in the field. Results for the other waveforms can be found in Appendix C.

Figure 5.6 shows the waveform that was analyzed. Run 1, Table 5.5, produced no RHP poles and therefore more pressure was required on the method. F2NYQ = 45 MHz was chosen, due to the frequency spectrum of the incident wave, and the largest possible number of poles was chosen for Run 2, Table 5.6. Here three RHP poles appeared, one almost a DC pole, and two at 8 MHz; therefore, less pressure must now be exerted at the same F2NYQ. In Run 3,

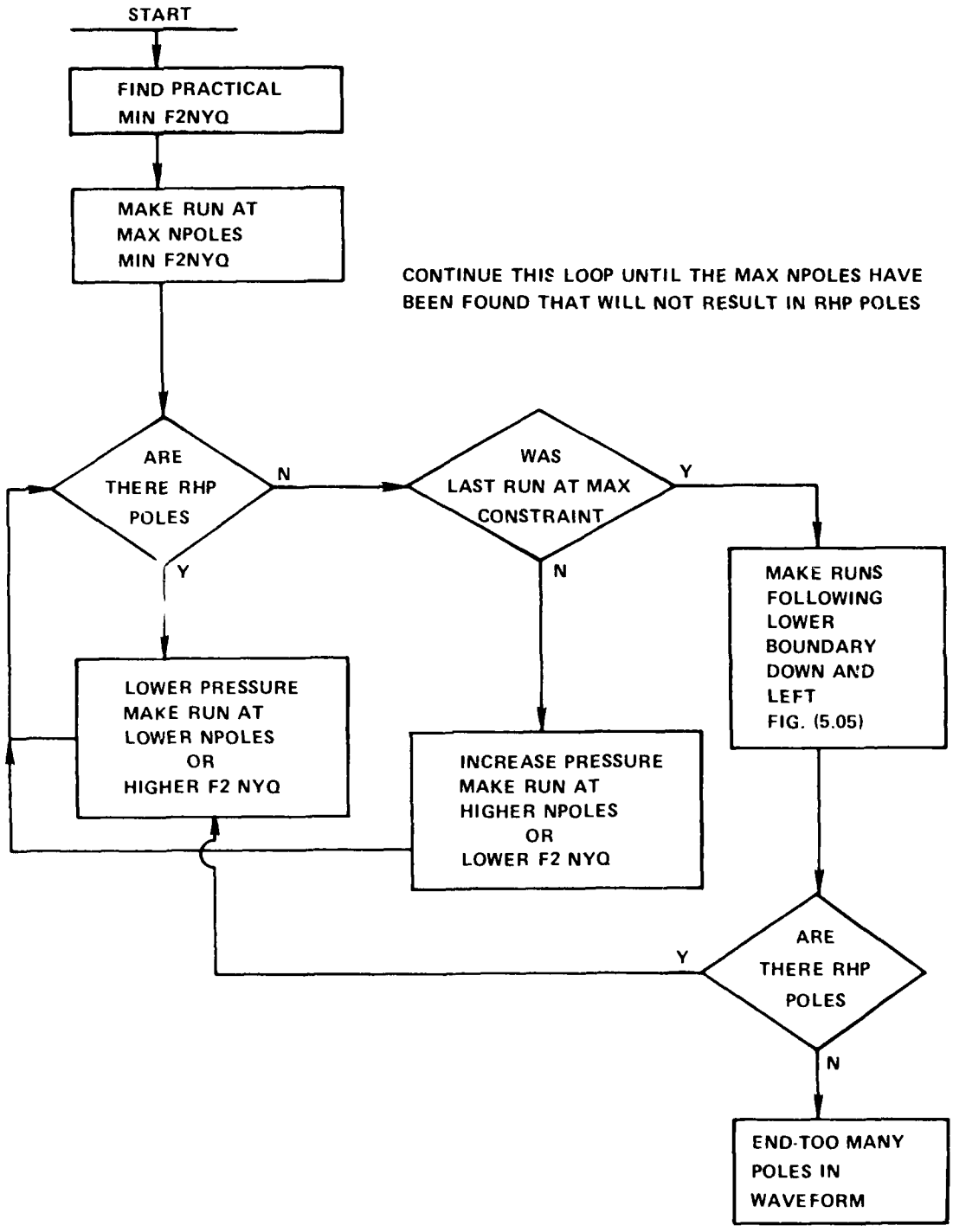

FIG. 5.4 NYQUIST CRITERION METHOD FLOWCHART

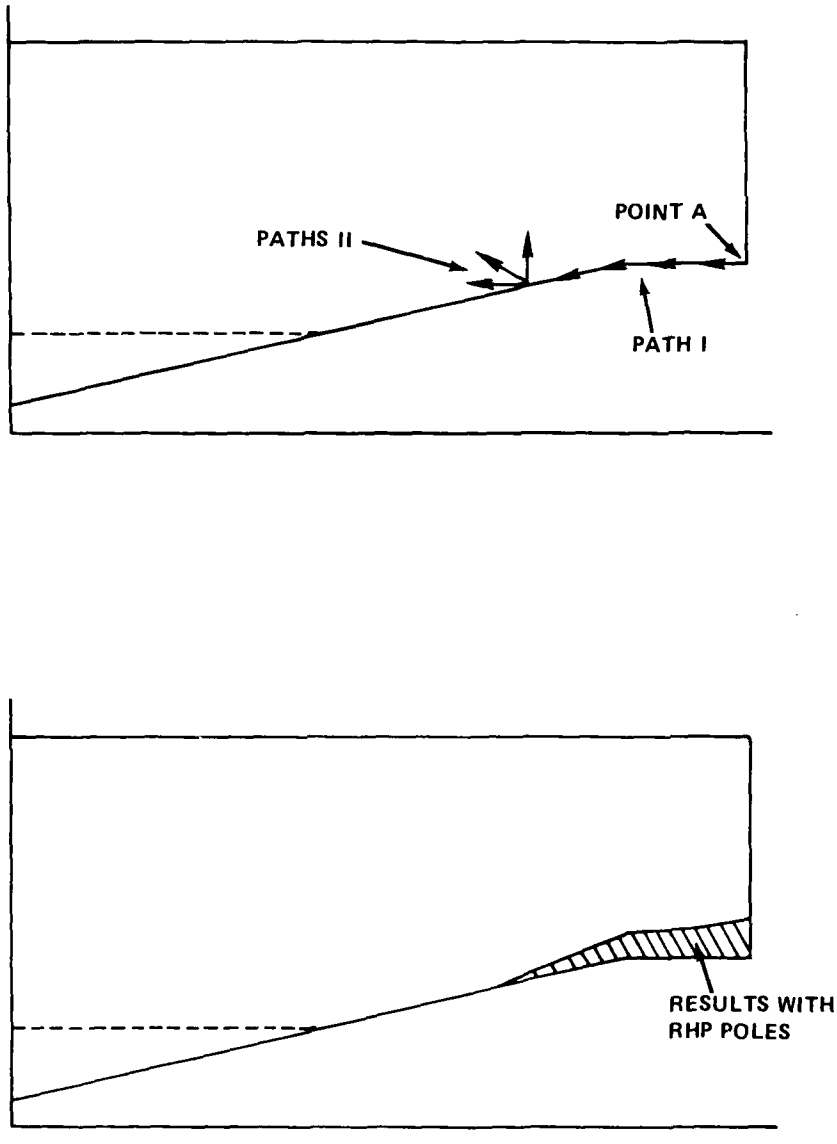

FIG. 5.5 USING THE NYQUIST CRITERION METHOD

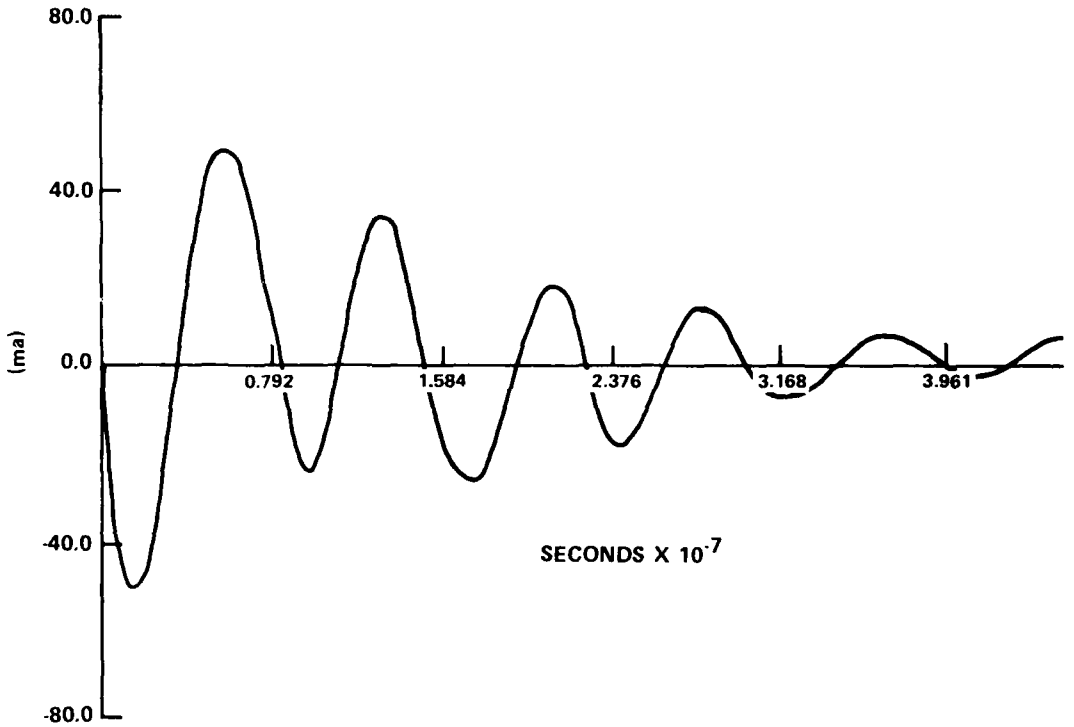

FIG. 5.6 WAVEFORM USED FOR RUNS (1-4)

Table 5.4. Waveform with Many Curve Fit Poles

	Magnitude of Residue (ampl)	Real Part of Pole Location (nepers)	Imaginary Part of Pole Location (Hz)
1.	.18425E+01	-.11616E+08	.37664E+07
2.	.18425E+01	-.11616E+08	-.37664E+07
3.	.86832E-01	-.69082E+06	.58896E+07
4.	.86832E-01	-.69082E+06	-.58896E+07
5.	.23597E+01	-.51145E+07	.12867E+08
6.	.23597E+01	-.51145E+07	-.12867E+08
7.	.47945E+00	-.23231E+07	.15017E+08
8.	.47945E+00	-.23231E+08	-.15017E+08
9.	.29887E+00	-.68426E+07	.19042E+08
10.	.29887E+00	-.68246E+07	-.19042E+08
11.	.82564E+00	-.13110E+08	.22739E+08
12.	.82564E+00	-.13110E+08	-.22739E+08
13.	.49439E-02	-.12831E+08	.28402E+08
14.	.49439E-02	-.12931E+08	-.28402E+08
15.	.19976E+00	-.18515E+08	.35210E+08
16.	.19976E+00	-.18515E+08	-.35210E+08
17.	.95372E-02	-.52623E+07	.43187E+08
18.	.95372E-02	-.52623E+07	-.43187E+08
19.	.37700E-01	-.90551E+07	.48322E+08
20.	.37700E-01	-.90551E+07	-.48322E+08
21.	.79331E-01	-.30643E+08	.48534E+08
22.	.79331E-01	-.30643E+08	-.48534E+08
23.	.68969E-02	-.79727E+07	.57972E+08
24.	.68969E-02	-.79727E+07	-.57972E+08
25.	.74462E-01	-.57905E+08	.59951E+08
26.	.74462E-01	-.57905E+08	-.59951E+08
27.	.46629E-02	-.78563E+07	.69014E+08
28.	.46629E-02	-.78563E+07	-.69014E+08
29.	.99962E-02	-.13692E+08	.75708E+08
30.	.99962E-02	-.13692E+08	-.75708E+08
31.	.68656E-02	-.14997E+08	.78163E+08
32.	.68656E-02	-.14997E+08	-.78163E+08
33.	.24910E-02	-.78867E+07	.83649E+08
34.	.24910E-02	-.78867E+07	-.83649E+08

Note the great number of poles with small residues whose imaginary part is above 35 MHz. More than half of the poles are thus classified.

Table 5.5. Run 1

	Magnitude of Residue (ma)	Real Part of Pole Location (neperes)	Imaginary Part of Pole Location (Hz)
1.	.34985E+01	-.19344E+08	.43716E+07
2.	.34985E+01	-.19344E+08	-.43716E+07
3.	.15853E+01	-.17377E+08	.69290E+07
4.	.15853E+01	-.17377E+08	-.69290E+07
5.	.33907E+01	-.69217E+07	.14317E+08
6.	.33907E+01	-.69217E+07	-.14317E+08
7.	.48341E+00	-.53880E+07	.17596E+08
8.	.48341E+00	-.53880E+07	-.17596E+08
9.	.85324E+00	-.11644E+08	.18579E+08
10.	.85324E+00	-.11644E+08	-.18579E+08
11.	.16288E+01	-.32862E+08	.25082E+08
12.	.16288E+01	-.32862E+08	-.25082E+08
13.	.13408E+00	-.19282E+08	.38361E+08
14.	.13408E+00	-.19282E+08	-.38361E+08
15.	.98865E-02	-.62617E+07	.47158E+08
16.	.98865E-02	-.62617E+07	-.47158E+08
17.	.29211E-01	-.76612E+07	.52787E+08
18.	.29211E-01	-.76612E+07	-.52787E+08
19.	.22518E+00	-.66557E+08	.58033E+08
20.	.22518E+00	-.66557E+08	-.58033E+08
21.	.71353E-02	-.89836E+07	.64131E+08
22.	.71353E-02	-.89836E+07	-.64131E+08
23.	.19278E-01	-.13249E+08	.75961E+08
24.	.19278E-01	-.13249E+08	-.75961E+08
25.	.21934E-01	-.16992E+08	.81596E+08
26.	.21934E-01	-.16992E+08	-.81596E+08
27.	.38825E-01	-.24262E+08	.87869E+08
28.	.38825E-01	-.24262E+08	-.87869E+08
29.	.88954E-02	-.81530E+07	.92629E+08
30.	.88954E-02	-.81530E+07	-.92629E+08
31.	.34823E-02	-.46219E+07	.10393E+09
32.	.32823E-02	-.46219E+07	-.10393E+09
33.	.73191E-02	-.10197E+08	.11443E+09
34.	.73191E-02	-.10197E+08	-.11443E+09

NPOLES = 34
NBEGN = 2
NPTS = 100

NDECI = 5
F2NYQ = 117.5 MHz
RMS ERROR = 8.72%

Table 5.6. Run 2

	Magnitude of Residue (ma)	Real Part of Pole Location (neperes)	Imaginary Part of Pole Location (Hz)
1.	.15006E-02	.12459E+08	.69945E-09
2.	.23807E+01	-.14536E+08	-.45008E+07
3.	.23807E+01	-.14536E+08	.45008E+07
4.	.32854E-01	.41202E+07	-.87541E+07
5.	.32854E-01	.41202E+07	.87541E+07
6.	.25443E+01	-.57049E+07	-.14098E+08
7.	.25443E+01	-.57049E+07	.14098E+08
8.	.46477E+00	-.30601E+07	-.16997E+08
9.	.46477E+00	-.30601E+07	.16997E+08
10.	.48234E+00	-.84151E+07	-.21333E+08
11.	.48234E+00	-.84151E+07	.21333E+08
12.	.12089E+01	-.19126E+08	-.25246E+08
13.	.12089E+01	-.19126E+08	.25246E+08
14.	.31278E-01	-.71038E+07	-.29891E+08
15.	.31278E-01	-.71038E+07	.29891E+08
16.	.69807E-01	-.12013E+08	-.39126E+08
17.	.69807E-01	-.12013E+08	.39126E+08
18.	.62090E-02	-.24492E+07	-.47464E+08
19.	.62090E-02	-.24494E+07	.47464E+08
20.	.43172E+00	-.43748E+08	-.48954E+08

NPOLES = 20
NBEGN = 2
NPTS = 42

NDECI = 12
F2NYQ = 48.95 MHz
RMS ERROR = 0.286%

Table 5.7, note that the RHP poles have disappeared, and a pole on the order of 5.7 MHz reappeared. This pole can be seen in Run 1, but it is missing in Run 2, thus showing the unreliability of results that contain RHP poles. It is also interesting to see that the inclusion of the RHP poles in Run 2 lowered the error of the reconstructed waveform by an order of magnitude. With even less pressure in Run 4, Table 5.8, the error is up a bit with all pole locations slightly shifted. As a check, many runs were made at F2NYQ with $4 \leq$ NPOLES ≤ 20 to see if the error at any other point dropped to a low level, indicating that the waveform might be adequately described by even fewer poles. The resulting curve is shown in Figure 5.7. Notice how the error drops significantly in the beginning up to NPOLES = 10, then levels out somewhat. It is here that more curve fit poles are being calculated than real poles.

Table 5.7. Run 3

	Magnitude of Residue (ma)	Real Part of Pole Location (nepers)	Imaginary Part of Pole Location (Hz)
1.	.21493E+01	-.13607E+08	.44044E+07
2.	.21493E+01	-.13607E+08	-.44044E+07
3.	.83460E-01	-.18361E+07	.62077E+07
4.	.83460E-01	-.18361E+07	-.62077E+07
5.	.26701E+01	-.66503E+07	.13923E+08
6.	.26701E+01	-.66503E+07	-.13923E+08
7.	.95226E+00	-.52590E+07	.16525E+08
8.	.95226E+00	-.52509E+07	-.16525E+08
9.	.68501E+00	-.11421E+08	.20655E+08
10.	.68501E+00	-.11421E+08	-.20655E+08
11.	.11797E+01	-.17158E+08	.25151E+08
12.	.11797E+01	-.17158E+08	-.25151E+08
13.	.91204E-01	-.17377E+08	.28695E+08
14.	.91204E-01	-.17377E+08	-.28695E+08
15.	.82218E-01	-.13772E+08	.39290E+08
16.	.82218E-01	-.13772E+08	-.39290E+08
17.	.46269E+00	-.29978E+08	.48594E+08
18.	.10687E+00	-.13574E+08	-.48594E+08

NPOLES = 18
NBEGN = 2
NPTS = 42

NDECI = 12
F2NYQ = 48.95 MHz
RMS ERROR = 7.23%

Table 5.8. Run 4

	Magnitude of Residue (ma)	Real Part of Pole Location (nepers)	Imaginary Part of Pole Location (Hz)
1.	.27729E+01	-.17377E+08	.40765E+07
2.	.27729E+01	-.17377E+08	-.40765E+07
3.	.15631E+01	-.19830E+08	.71158E+07
4.	.15631E+01	-.19830E+08	-.71158E+07
5.	.40284E+01	-.79235E+07	.14295E+08
6.	.40284E+01	-.79235E+07	-.14295E+08
7.	.13182E+01	-.97781E+07	.17612E+08
8.	.13182E+01	-.97781E+07	-.17612E+08
9.	.36972E+01	-.33842E+08	.21366E+08
10.	.36972E+01	-.33842E+08	-.21366E+08
11.	.13981E+01	-.14187E+08	.23880E+08
12.	.13981E+01	-.14187E+08	-.23880E+08
13.	.11507E+00	-.16169E+08	.38732E+08
14.	.11507E+00	-.16169E+08	-.38732E+08
15.	.12225E+00	-.18730E+08	.46431E+08
16.	.12225E+00	-.18730E+08	-.46431E+08

NPOLES = 16
NBEGN = 2
NPTS = 42

NDECI = 12
F2NYQ = 48.95 MHz
RMS ERROR = 8.79%

FIG. 5.7 RECONSTRUCTED WAVEFORM ERROR VERSUS NUMBER OF POLES REQUESTED

CHAPTER 6

CONCLUSIONS AND RECOMMENDATIONS

6.1 CONCLUSIONS

This work has shown that Prony's method is a possible experimental data reduction technique. The Nyquist Criterion Constraint method proposed, provides a limit on the possible number of real poles in a system within a given bandwidth. The lower limit is provided by the length of the waveform recorded, and the upper limit of the bandwidth is set by the dominant frequencies in the waveform with respect to a Nyquist rate. The process of windowing can be used with some success to try to eliminate the curve fit poles but in general all poles shift about from run to run. These shifts can be observed mostly in the real part of the pole location. Van Blaricum[17] showed that the real part is more susceptible to noise, by making many runs with several waveforms all corrupted by various levels of "random" noise, from 2 dB to 49 dB signal to noise ratios. Using Prony's method on response waveforms taken aboard a ship is therefore a questionable proposition at this time. It would be very useful for the cleaner, simpler waveforms that can be recorded on or near the mast and its cables; but for the analysis of scattered fields as done here, the waveforms are too noisy and cause great inaccuracy and concern. Identification of some of the real poles can be accomplished by simple calculations and the locations of the others must for now be simply accepted as given in the runs. There still is no good way to eliminate the curve fit poles from the results. In its present form this method provides useful poles of transient responses and certainly provides an excellent way to store data in about 10% to 20% of space required for a digitized waveform.

6.2 RECOMMENDATIONS

Noise reduction should be the primary concern. Some aspects of it could include meticulous digitization practices, a study of the numerical procedures, their contributions to and effects upon noise in the waveform. Examples are, deconvolution, types of filtering, and transformations. Some preliminary work has already been done.

but none as yet seems to be a good technique[17,32,35]. The SEMPEX code should be trimmed down; it should be possible to cut down the size of needed core by tens of K. This would provide enough space for the calculation of more poles as was seen necessary from the experiments dealing with the scattering from the sewer pipe (Appendix C). The possibility of averaging many runs together should be done numerically on the computer. In this way it would be possible to specify the size and shape of the area in the s-plane within which the poles will be averaged. For instance, ellipses should be used instead of circles, since it is known that the real part of the pole is subject to more shifting.

There is certainly great room for improvement in this area since not much work has been accomplished in methods for the identification of the real poles of a system. First the Nyquist Criterion should be further examined for usefulness, especially in cases where the response is clearly bandlimited in frequency. Also there may be some answers in observing the effects of sub-Nyquist rate sampling in the pole locations. The idea of forcing Prony's method to contain some known poles[19] has already been proposed by Van Blaricum[36], by forcing the response function to contain the poles of the driver. The Prony method should also be examined for use with Class II coefficients, and perhaps in the description of the ignored entire function; these two elements should also be examined in depth for use in better waveform representation. A study of pole movement should be considered for the case where finite objects are brought into the proximity of each other.

Singularity extraction from the time domain response waveform has great promise, for its applications are very powerful, but the root of all evil - the method's sensitivity to noise, must be dealt with before significant progress can be made in the process of correctly indentifying the real poles of the excited system.

REFERENCES

1. IIT Research Institute, Defense Nuclear Agency EMP Awareness Course Notes, DNA 2772 T, Aug 1971.

2. A. S. Leveckis, "EMP Coupling Through Apertures," Bachelor's Thesis, MIT, May 1976.

3. C. E. Baum, "The Singularity Expansion Method," in Transient Electromagnetic Fields, L. B. Felsen, Ed. Springer, New York, 1976, Chapter 3.

4. W. C. Emberson and R. H. Hueneman, NOL431-69001, "Preliminary Study of Time-Domain Measurement of Antenna Parameters," Jun 1970.

5. H. C. Pocklington, "Electrical Oscillations in Wires," Proc. Cambridge Phil. Soc., vol. 9, pp. 324-332, 1897.

6. C. W. Oseen, "Uber die elektischen Schwingungen an dunnen Staben," Arkiv Mat. Astr. Fysik. Vol. 9, no. 30, pp. 1-27, 1914.

7. E. Hallen, "Theoretical Investigations into the Transmitting and Receiving Antennae," Nova Acta Reg. Soc. Sci. Upsaliensis, vol. 11, no. 4, pp. 1-44, 1938.

8. K. K. Mei, "On the Integral Equations of Thin Wire Antennas," IEEE Trans. on Ant. and Prop., pp. 374-378, May 1965.

9. L. Marin, "Natural Modes of Certain Thin Wire Structures," Interaction Note No. 186, AFWL, Albuerque, NM, Aug 1974.

10. L. Marin, "Natural Mode Representation of Transient Scattering from Rotationally Symmetric Bodies and Numerical Results for the Prolate Spheroid," Interaction Note No. 119, AFWL, Albuquerque, NM, Sep 1972.

11. E. K. Miller, A. J. Poggio, and G. J. Burke, "An Integro Differential Technique for the Time-Domain Analysis of Thin Wire Structures, I. Numerical Results," in J. of Comp. Phys., vol. 12, pp. 24-48, 1973.

12. C. E. Baum, "Electromagnetic Transient Interaction with Obects with Emphasis on Finite Size Objects, and Some Aspects of Transient Pulse Production," Spring 1972 URSI Meeting, Washington, D. C., 1972.

13. F. Tesche, "On the Analysis of Scattering and Antenna Problems Using the Singularity Expansion Technique," IEEE Trans. APS, No. 1, 1973.

14. R. F. Harrington, Field Computation by Moment Methods, The MacMillan Co., New York, 1968.

15. R. V. Churchill, Complex Variables and Applications, McGraw-Hill Co., New York, 1960.

16. M. L. Van Blaricum and R. Mittra, "A Technique for Extracting the Poles and Residues of a System Directly from Its Transient Response," Interaction Note 245, AFWL, Albuquerque, NM, Feb 1975.

17. M. L. Van Blaricum, "Techniques for Extracting the Complex Resonances of a System Directly from Its Transient Response," PhD Dissertation, University of Illinois, 1976.

18. R. Prony, "Essai Experimental et Analytique sur les lois de la Dilatabilite de Fluides Elastiques et sur Celles del la Force Expansive de la Vapuer de l'alkool, a Differentes Temperatures," J. l'Ecole Polytech, vol. 1, no. 2, pp. 24-76, Parix, 1795.

19. F. B. Hildebrand, Introduction to Numerical Analysis, McGraw-Hill Co., New York, 1974, pp. 457-462.

20. J. D. Lawrence, "Polynomial Root Finder," LLL, Livermore, CA, CIC Rep. C212-001, Dec 1966.

21. M. S. Corrington, "Simplified Calculation of Transient Response," Proc. IEEE, vol. 53, Mar 1965, pp. 287-292.

22. K. L. Su, Time-Domain Synthesis of Linear Networks, Prentice Hall, Englewood Cliffs, NJ, 1971, pp. 23-26.

23. J. N. Brittingham, E. K. Miller, and J. L. Willows, "The Derivation of Simple Poles in a Transfer Function from Real-Frequency Information," UCRL-52050, LLL, Livermore, CA, Apr 1976.

24. J. N. Brittingham, E. K. Miller, and J. L. Willows, "The Derivation of Simple Poles in a Transfer Function from Real-Frequency Information, Part 2: Results from Real EM Data," UCRL-52118, LLL, Livermore, CA, Aug 1976.

25. J. N. Brittingham, E. K. Miller, and J. L. Wilson, "The Derivation of Simple Poles in a Transfer Function from Real-Frequency Information, Part 3," UCRL 52211, LLL, Livermore, CA, Jan 1977.

26. D. L. Moffatt and R. K. Mains, "Detection and Discrimination of Radar Targets," IEEE Trans. APS, vol. 23, no. 3, 1975, pp. 358-367.

27. G. Carrier, M. Krook, and C. Pearson, Functions of a Complex Variable, McGraw-Hill, New York, 1966.

28. C. E. Baum, "The Singularity Expansion Method," in Transient Electromagnetic Fields, L. B. Felsen, ed., Springer, New York, 1976, chapter 3.

29. E. M. Tesche, "Application of the Singularity Expansion Method to the Analysis of Impedance Loaded Linear Antennas," Sensor and Simulation Note 177, AFWL, Albuquerque, NM, May 1973.

30. D. L. Lager, H. G. Hudson, and A. J. Poggio, "User's Manual for SEMPEX," LLL, Livermore, CA, 1976.

31. F. B. Hildebrand, Introduction to Numerical Analysis, McGraw-Hill Co., New York, 1974, pp. 545-549.

32. D. L. Lager, A. J. Poggio, and H. G. Hudson, "Suppressing Some Noise Difficulties in Prony Processing," presented at USNC/URSI Conference, Amherst, MA, 1976.

33. R. J. Haislmaier, "The Electromagnetic Pulse Radiation Environment Simulator for Ships (EMPRESS)", presented at NATO EMC Workshop, Naval Air Test Center, Patuxent, MD, 1976.

34. E. J. Nicosia, "Requirements, Tasks, and Attributes of EMP Data Management," NSWC/WOL/TR 75-25, Feb 1975.

35. D. G. Dudley, "Random errors in Prony's Method," presented at USNC/URSI Conference, Amherst, MA, 1976.

36. M. L. Van Blaricum, "A Method for the Analysis of EMP Simulator Data," MRC, Santa Barbara, CA, Dec 1976.

APPENDIX A

COMPARISON OF THE TIME AND FREQUENCY DOMAIN PRONY TECHNIQUES

	Time Domain	Frequency Domain
Defining equation	$f(t) = \sum_{i=1}^{N} R_i e^{s_i t}$	$F(s) = \sum_{i=1}^{N} \frac{R_i}{s - s_i}$
Rearrange equation (superscript denotes the absence of the i=j term)		$F(s) = \prod_{i=1}^{N} s-s_i = \sum R_i \prod_{j=1}^{Ni} (s-s_j)$
Introduce polynomial expansion	$\sum_{i=0}^{N} a_i X^i; \quad a_N=1$ $X = e^{s\delta}$	$\sum_{i=0}^{N} a_i s^i; \quad a_N=1$ $\sum_{j=0}^{N-1} b_j^i s^j; \quad b_{N-1}^i$
Sample data	$f_k = f(p\delta); \quad p=0,..,N$ (note: equally spaced samples)	$F_k = F(s_k); \quad k=o,...,N$ (note: samples can be arbitrarily spaced)
Develop linear system for polynomial coefficients	$\sum_{i=0}^{N-1} N_{ki} a_i = -f_{n+k}$ $N_{ki} = f_{k+i}$ $i = 0,....,N-N$ (system has N real unknowns and N+1 2N)	$\sum_{i=0}^{N-1} (N_{ki} a_i - N_{ki} \tilde{b}_i) = -s_k^N F_k$ $N_{ki} = s_k^i F_k$ $N_{ki} = s_k^i; \; i = 0,...,N$ $\tilde{b}_j = \sum R_i b_j^i$ (system has 2N real unknowns and N+1 N)
Find poles s_i from	$\sum_{j=0}^{N} a_j x_i^j = 0$ $s_i = \frac{1}{\delta} \ln X_i \quad i=1,..,N$	$\sum_{j=0}^{N} a_j s_i^j = 0$ $i = 1,...,N$
Find residues R_i from	$\sum_{i=1}^{N} N_{ki} R_i = f_k$ $N_{ki} = X_k^i; \; i=1,..N,..,N$	$\sum_{i=1}^{N} N_{ki} R_i = F_k$ $N_{ki} = \frac{1}{s_k - s_i}; \; i=0,...,N,..N$

APPENDIX B

CHARACTERISTICS OF THE EMPRESS ELECTRIC FIELD

Given a cylindrical coordinate system (r,θ,z) with $r = z = 0$ at the pulser, the components of the vertically polarized electric field, as measured with the B-dot sensor, at the anchor point in the interaction area are:

Measurement	Field Strength (kV/m)	Percentage of Principal Component
E_z	2.7	100%
E_θ	.174	6.4%
E_r	.27	10%

The peak electric field versus distance from EMPRESS as measured with the B-dot sensor are: (see Figure B.1)

Location	Peak Field Strength (V/m)	Distance (m)
#1 Anchor Point	2700	350
#2 Near Bridge	1000	1100
#3 Off Solomons Pier	420	2200
#4 Buoy - 8	270	3300
#5 Buoy - 6	130	4100

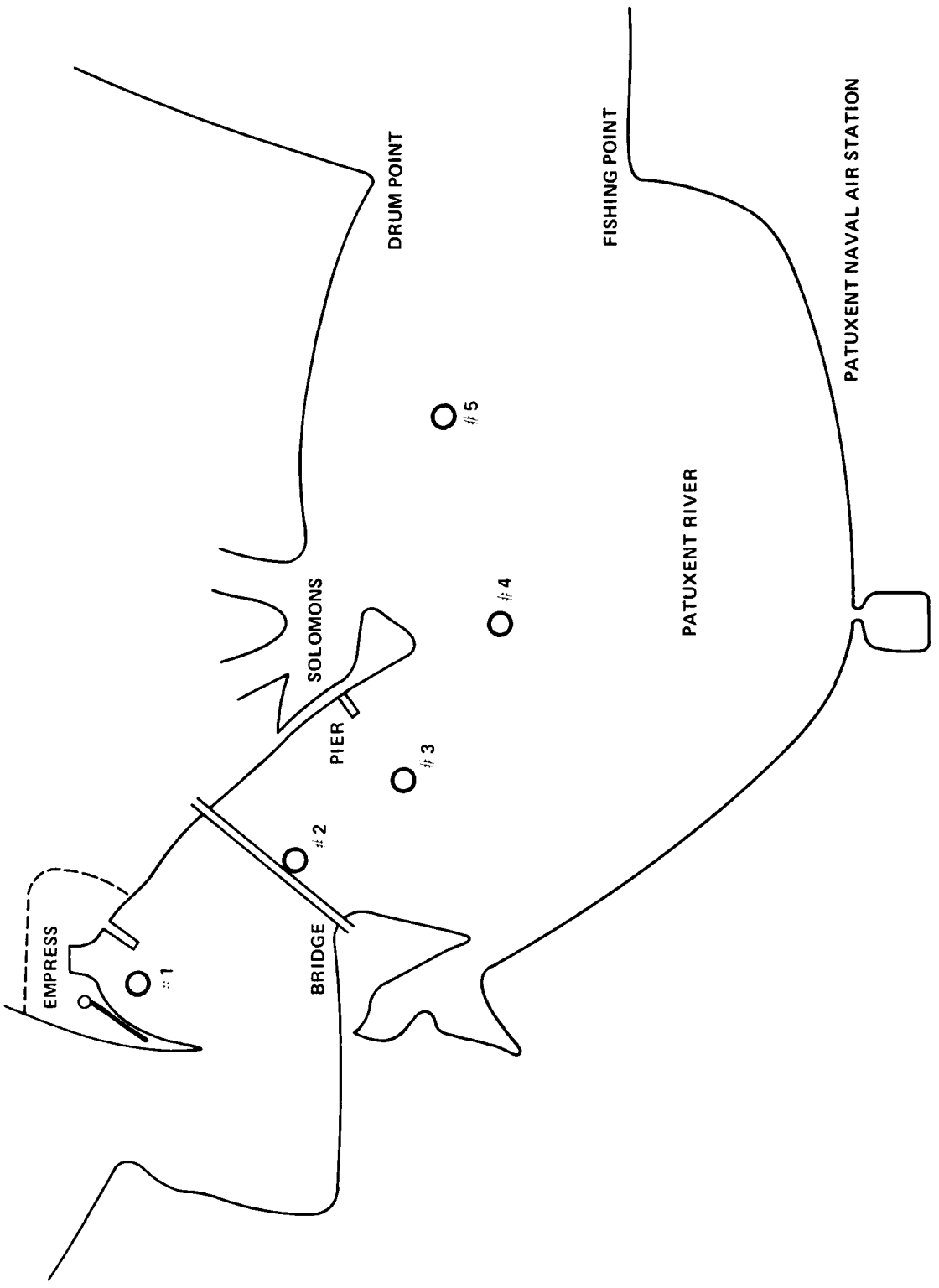

FIG. B.1 FIELD MEASUREMENT POINTS DOWNRIVER FROM EMPRESS

APPENDIX C

RESULTS OF THE FOUR TEST CASES

Many runs were made of the four test waveforms. Here, are presented the results. Pictured are: the waveforms, the rms error of the reconstructed waveform and the pole plot arrived at by averaging the results of the runs. As can be seen, some poles can be confirmed initially by a Fourier transform and later in their recurrent appearances from test case to test case. RHP poles could not be forced out in the runs of Test #3 and #4. This is due to the extra poles that are introduced into the system when the sewer pipe is presented as a scatterer in the field. An interesting note is that the 4.5 MHz pole of the pulser vanished when the AS 1018 receiving antenna was on the shadow side of the cylinder, as in Test #4.

The Test #2 waveform has already been analyzed in Tables 5.5 through 5.8 and Figures 5.6 and 5.7 here in addition is presented the pole plot of the waveform.

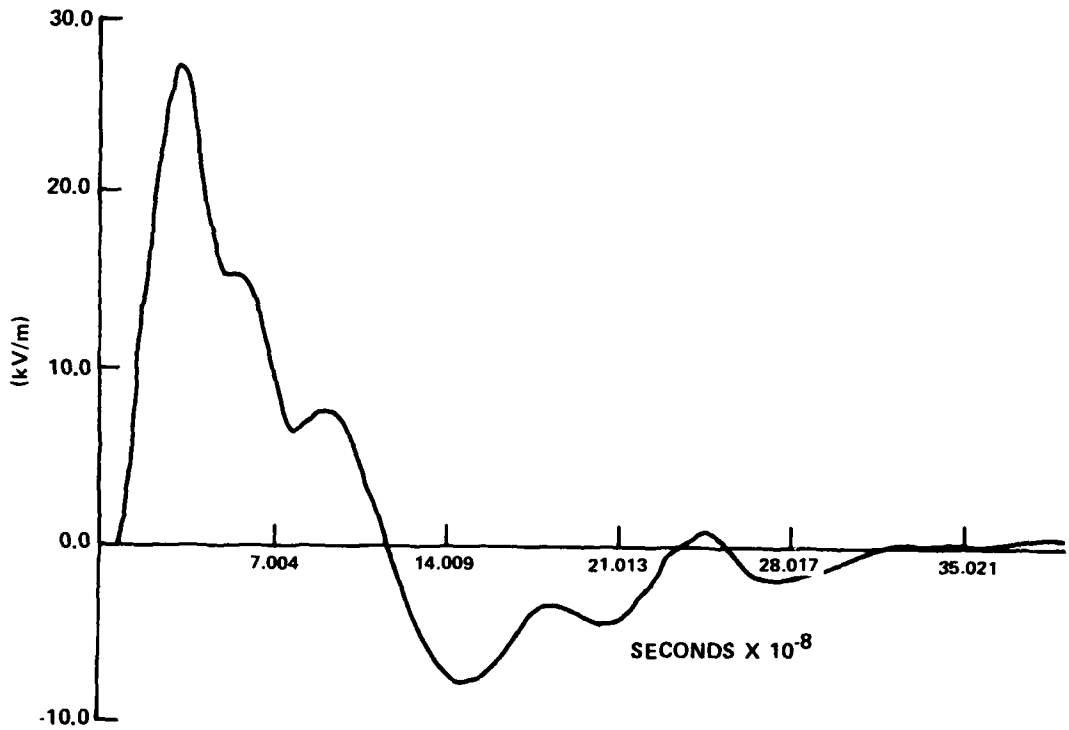

FIG. C.1 TEST NO. 1 WAVEFORM

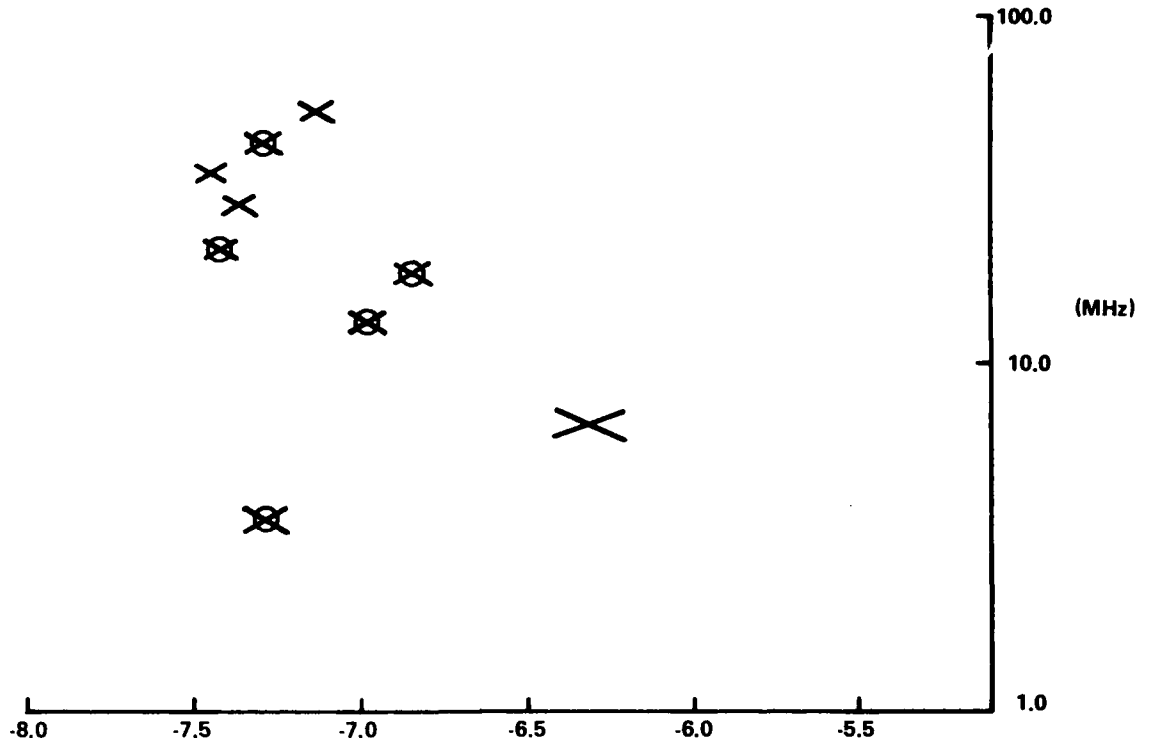

FIG. C.2 POLE PLOT OF TEST NO. 1 WAVEFORM

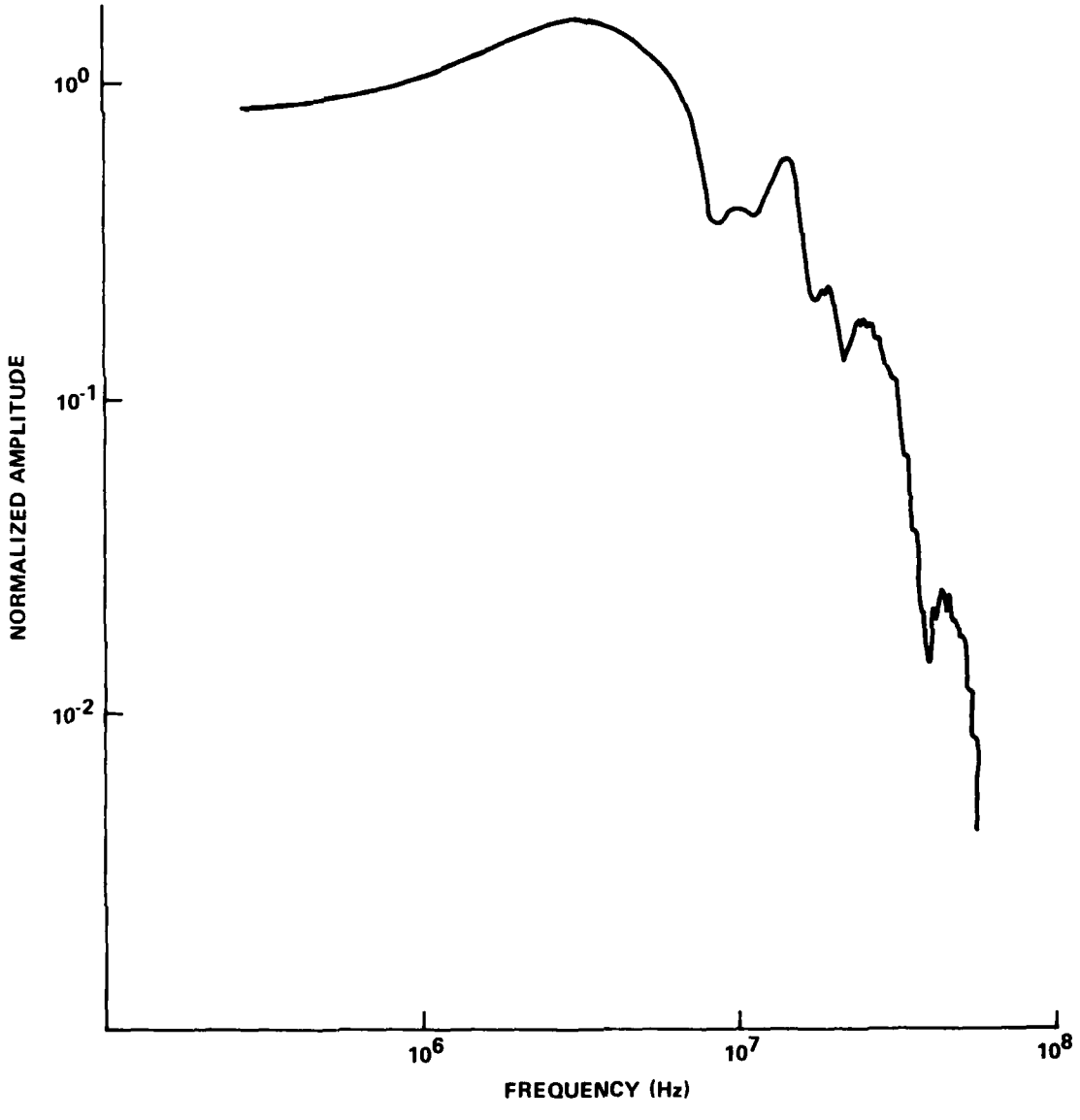

FIG. C.3 FOURIER TRANSFORM OF TEST NO. 1 WAVEFORM

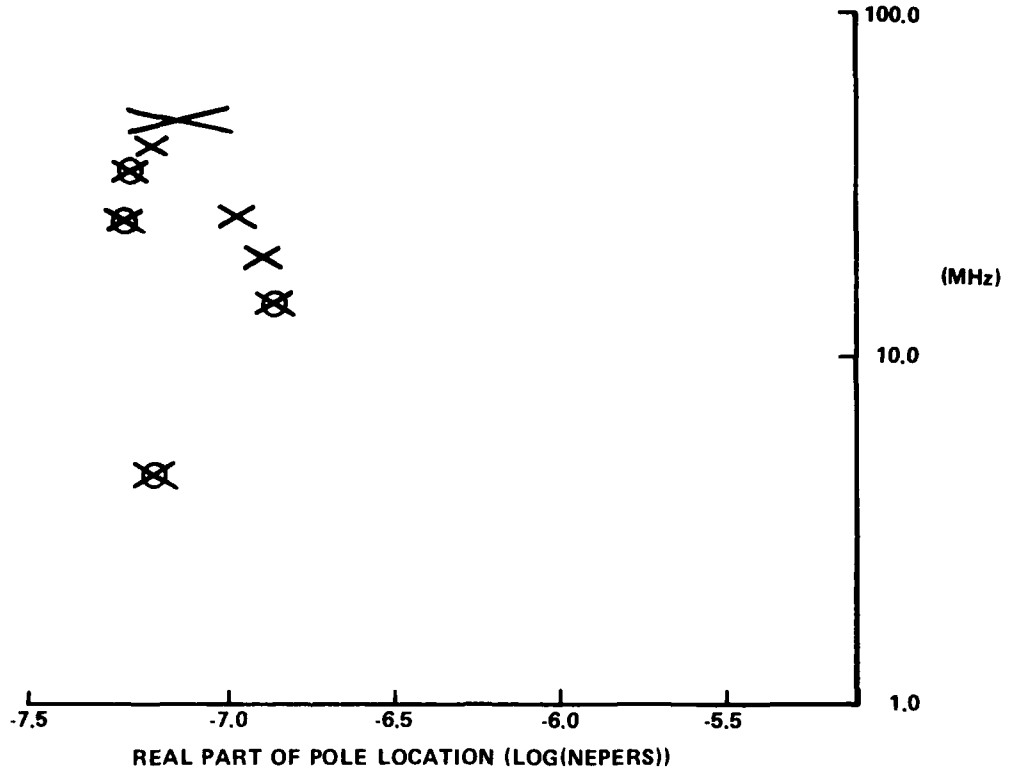

× POLE IDENTIFIED BY AVERAGING SEVERAL RUNS

⊗ POLE CONFIRMED BY EITHER FOURIER TRANSFORM OR APPEARANCE IN OTHER POLE PLOTS

FIG. C.4 POLE PLOT OF TEST NO. 2 WAVEFORM

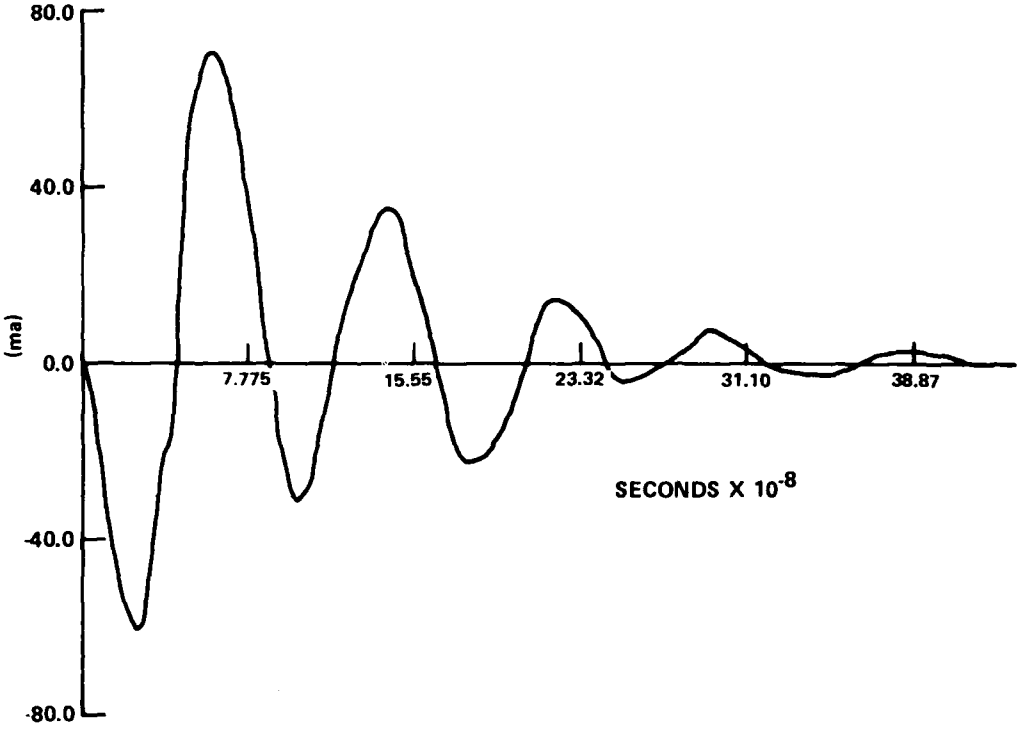

FIG. C.5 TEST NO. 3 WAVEFORM

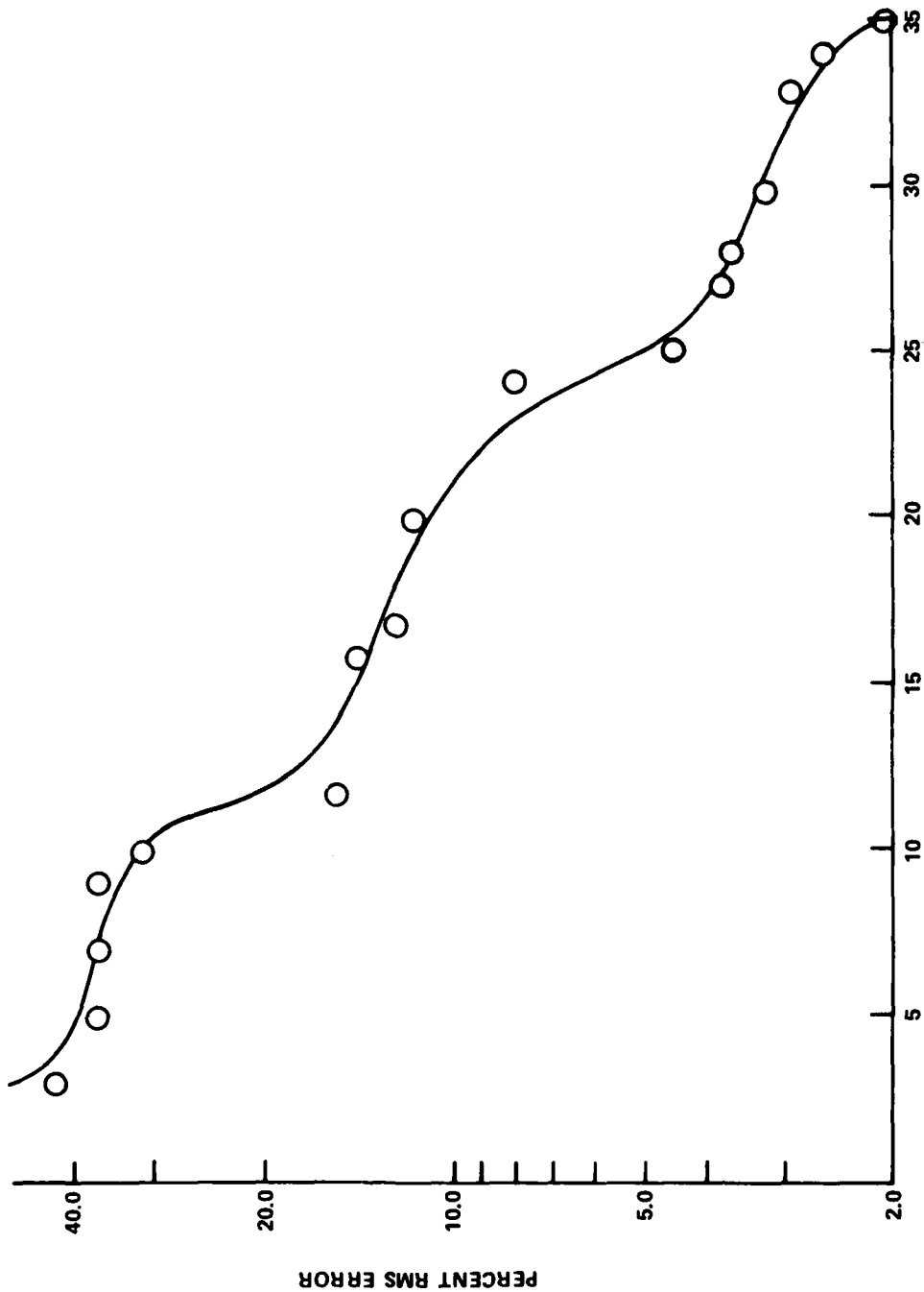

FIG. C.6 TEST NO. 3 WAVEFORM, RMS ERROR VERSUS NPOLES

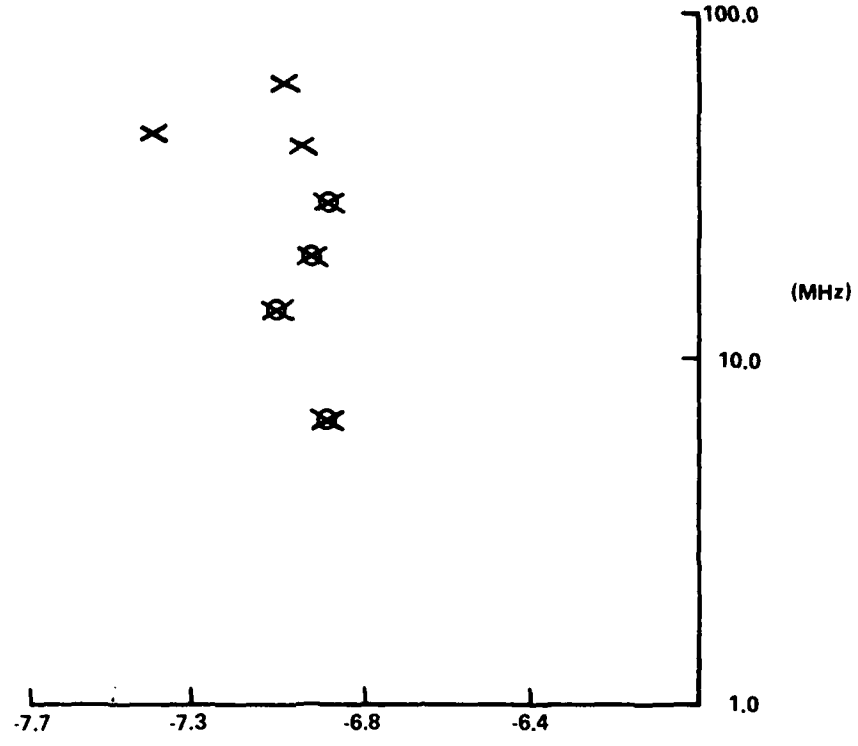

FIG. C.7 POLE PLOT OF TEST NO. 3 WAVEFORM

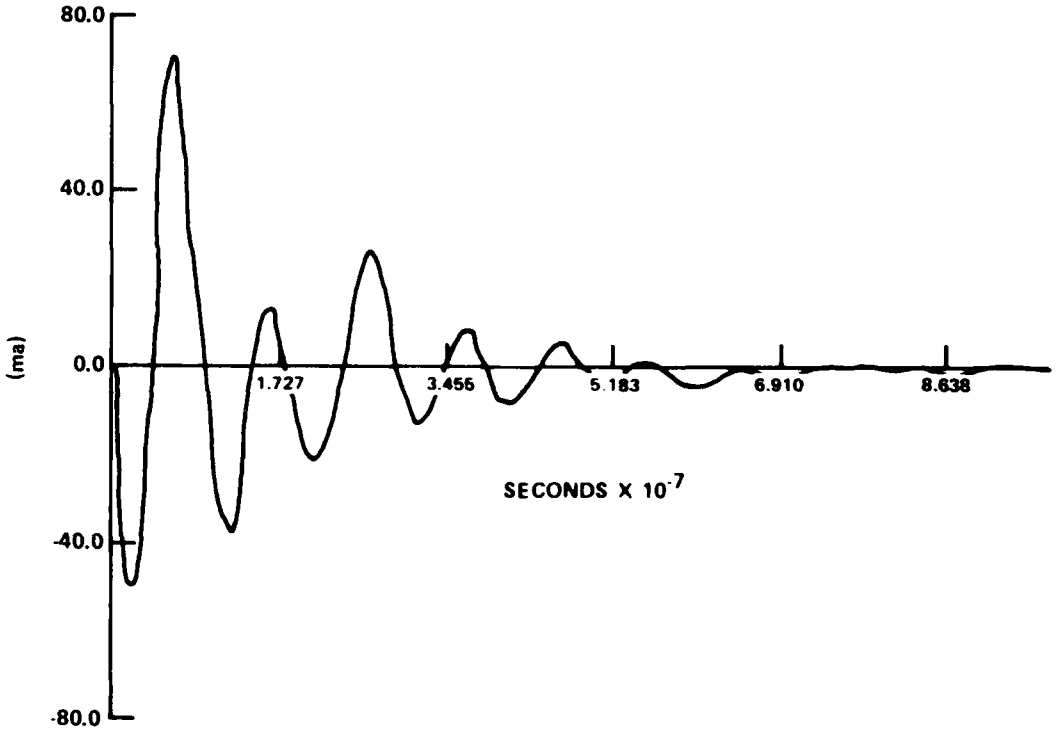

FIG. C.8 TEST NO. 4 WAVEFORM

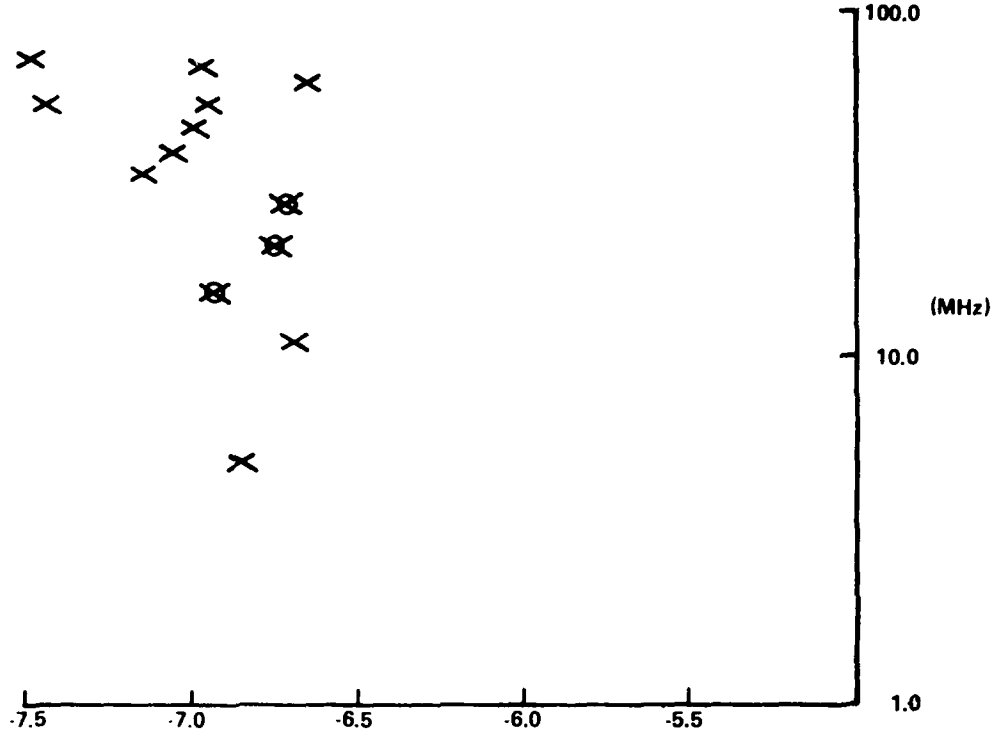

× POLE IDENTIFIED BY AVERAGING SEVERAL RUNS

⊗ POLE CONFIRMED BY EITHER FOURIER TRANSFORM OR APPEARANCE IN OTHER POLE PLOTS

FIG. C.9 POLE PLOT OF TEST NO. 4 WAVEFORM

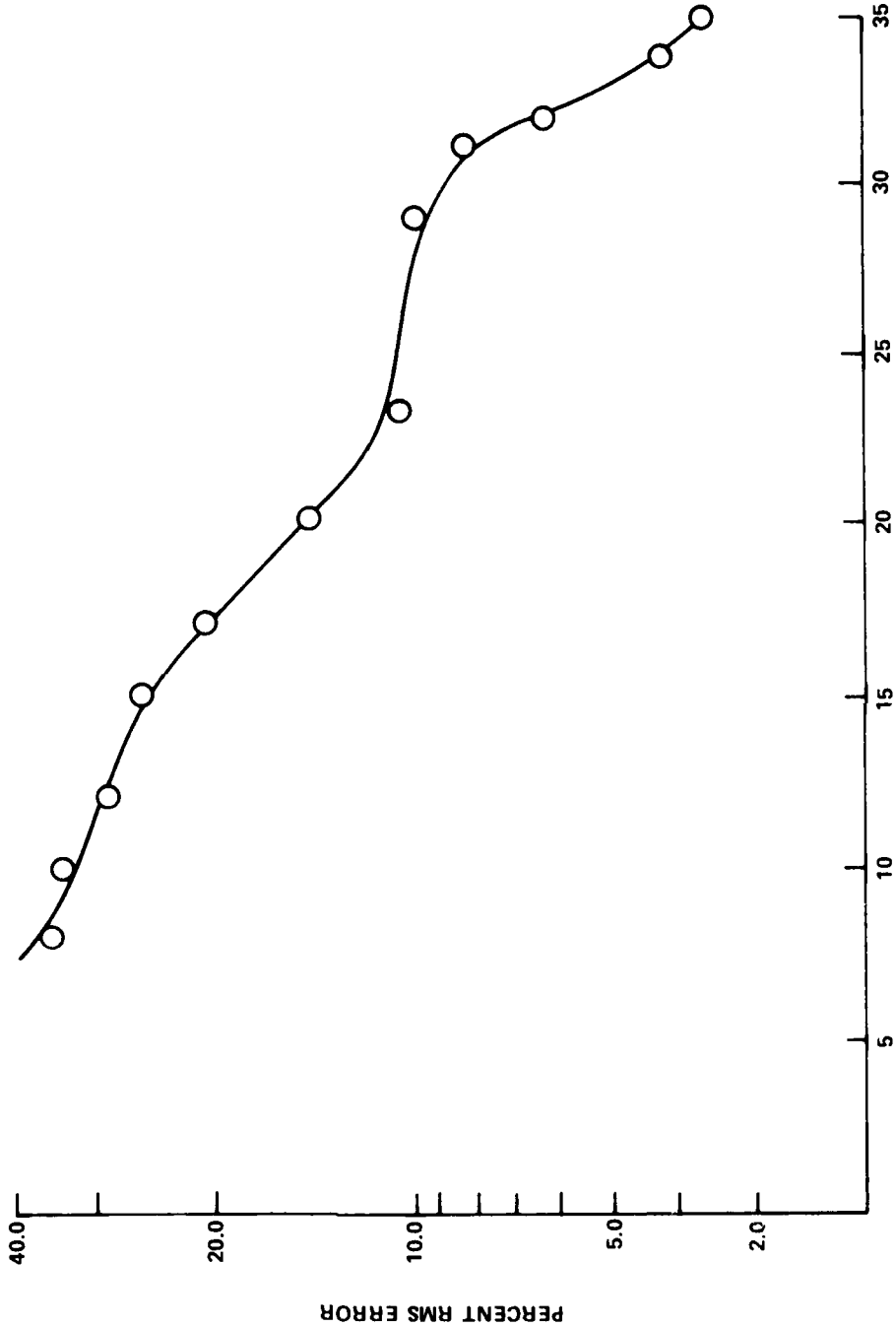

FIG. C.10 TEST NO. 4 WAVEFORM, RMS ERROR VERSUS NPOLES

DISTRIBUTION

Assistant to the Secretary of Defense
(Atomic Energy)
Attn: Document Control
Washington, DC 20301

Director
Defense Nuclear Agency
Attn: APTL, Technical Library
RAEV (G. Baker)
Washington, DC 20305

Director of Defense Research and Engineering
Attn: Technical Library
Washington, DC 20301

Chief
Livermore Division, Field Command, DNA
Lawrence Livermore Laboratory
Attn: Document Control
Box 808
Livermore, CA 94550

Assistant Secretary of the Navy
(Research & Development)
Attn: Document Control
Washington, DC 20301

Commander
Naval Electronic Systems Command
Headquarters
Attn: Technical Library
Washington, DC 20360

Chief of Naval Operations
Department of the Navy
Attn: Technical Library
Washington, DC 20350

Commander
Operational Test and Evaluation Force
Attn: Document Control
Code 02T (CDR K. McBride)
Norfolk, VA 23511

DISTRIBUTION (Continued)

Chief of Naval Research
Department of the Navy
Attn: Document Control
800 North Quincy Street
Arlington, VA 22217

Commander
Naval Air Systems Command
Headquarters
Attn: Technical Library
Washington, DC 20361

Chief of Naval Material
Department of the Navy
Attn: Technical Library
MAT-08T223 (F. Romano)
MAT-08DE (N. Jackson)
Washington, DC 20360

Director
Naval Research Laboratory
Attn: Technical Library
Washington, DC 20375

Commander
Naval Ocean Systems Center
Attn: Technical Library
San Diego, CA 92152

Commander
Naval Weapons Center
Attn: Technical Library
China Lake, CA 93555

Commander
Naval Sea Systems Command
Attn: Technical Library
Washington, DC 20362

Defense Technical Information Center
Cameron Station
Alexandria, VA 22314 (12)

Library of Congress
Washington, DC 20540
Attn: Gift & Exchange Division (4)

DOE Operations Office
Pasadena, CA 91720

Local

E41
F30
F32
F32 (Brackett)
F32 (Carroll)
F32 (Koury)
F32 (Stetson)
R43 (Libelo)
S30 (Weinert)
X210 (6)
X211 (2)


D
FI
8